Cryogenic Characterization of Josephson Junctions

by

Keith Andrew Brown

Submitted to the Department of Physics
in partial fulfillment of the requirements for the degree of

Bachelor of Science in Physics

at the

MASSACHUSETTS INSTITUTE OF TECHNOLOGY

May 2006
[June 2006]

© Massachusetts Institute of Technology 2006. All rights reserved.

Author .....
Department of Physics
May 18, 2006

Certified by .....
Leonid Levitov
Professor
Thesis Supervisor

Certified by .....
William D. Oliver
MIT Lincoln Laboratory
Thesis Supervisor

Accepted by .....
David E. Pritchard
Senior Thesis Coordinator, Department of Physics

MASSACHUSETTS INSTITUTE OF TECHNOLOGY
JUL 07 2006
LIBRARIES
ARCHIVES

Cryogenic Characterization of Josephson Junctions

by

Keith Andrew Brown

Submitted to the Department of Physics
on May 18, 2006, in partial fulfillment of the
requirements for the degree of
Bachelor of Science in Physics

Abstract

Cryogenic characterization is a crucial part of understanding the behavior of low-temperature quantum electronics. Reliable device testing provides the feedback to fabrication process development, facilitating the rapid development of quantum devices. The research presented in this thesis explores the cryogenic testing, analysis, and characterization of a superconducting quantum device, the Josephson junction. This thesis begins with a theoretical description of superconductivity and Josephson junctions, two superconductors separated by a thin insulating battier. Two models of Josephson barriers are presented for use in analysis. The effect of self-induced magnetic field is considered. A numerical simulation is performed to justify neglecting effects of self-induced magnetic field in junctions of diameter less than the Josephson penetration depth λ_J. Lincoln Laboratory's Josephson junction fabrication effort is described along with the apparatus used to test junctions at 4.2 K. Custom software used to test these junctions is then presented. The analysis of 4.2 K data is shown with a simple model of a disc as the insulating barrier. 391 valid Josephson junctions are analyzed across 16 wafers in 3 runs. The critical current density J_c is calculated to be 4.88 ± 2.81 $(\frac{\mu A}{\mu m^2})$ for junctions with expected J_c of 5 $(\frac{\mu A}{\mu m^2})$. The superconductive energy gap Δ is calculated to be 1.51 ± 0.31 meV. The process bias δ_0 is shown to be -0.35 ± 0.12 μm. Analyzing the junctions with an alternate model taking into account pollution produces an upper bound for barrier pollution depth of approximately 60 nm. Discussion of a 300 mK apparatus is then presented. This apparatus is constructed and presently being incorporated in an existing 300 mK ^{3}He refrigerator. Finally, the results are concluded with a discussion of advantages, and proposed initial experiments for the 300 mK apparatus.

Thesis Supervisor: Leonid Levitov
Title: Professor

Thesis Supervisor: William D. Oliver
Title: MIT Lincoln Laboratory

Acknowledgments

I would like to acknowledge many people for their contributions to my thesis. First, my advisor at Lincoln Laboratory, Dr. William Oliver, has been extraordinarily helpful and patient. I owe him my deepest gratitude for his continual help and advice about this thesis and more. Terry Weir, Robert Konieczka, and JoAnne Rantz have been very helpful, and I thank them for their technical help, advice, and company. I would like to thank Vladimir Bolkhobsky for his help as well. On campus, Prof. Terry Orlando was very helpful and welcoming as I worked through the simulation. I would like to thank Janice Lee for her help with theory. David Berns deserves my thanks for his patience and help with laboratory and apparatus design. Prof. Leonid Levitov also deserves my thanks for his feedback on my thesis. I would also like to thank the MIT machine shop and Peter Morley in particular for their patience in dealing with someone who had never done design before. I would like to thank peers who helped me through technical difficulty, Mike Wolf, Victor Brunini, Sam Raymond and Matthew Drake. Finally I would like to thank my friends and family that sympathized and supported me during this project.

Contents

List of Figures

List of Tables

Chapter 1

Theory and Motivation

1.1 Motivation

The Josephson effect is the physical effect that describes tunneling between two superconductors through an insulator i.e., a Josephson junction. The Josephson junction has been an important device in quantum electronics since it was predicted in 1962 by Brian David Josephson [1]. The properties of Josephson junctions and Josephson-based devices have made them of particular interest to the areas of precise magnetic sensing, quantum computing, superfluidity, and solid state physics. These properties include extreme sensitivity to magnetic fields, a small voltage-free dissipationless supercurrent, and nonlinearity in resistance.

Josephson junctions have been used as constituents of Superconductive Quantum Interference Devices (SQUIDs) which are used to measure magnetic fields with very high sensitivity [2]. High resolution probes for detecting magnetic fields have been implemented with SQUIDs with spatial resolution of 10 μm [3]. This has also been implemented in Niobium systems operated at 4.2 K [4]. SQUID based magnetic imaging has been used to detect nuclear magnetic resonance (NMR) and biomagnetic signals at ultra-low fields [5].

Josephson junctions can be used as the building blocks of logic elements for Quantum Computation. Persistent current quantum bits (qubits) are a convenient and readily fabricated type of qubit that can be magnetically coupled to an outside system

[6]. Multiple qubit systems have been fabricated out of charge-based and flux-based qubits comprised of Josephson junctions [7]

The Josephson effect has been observed in systems besides superconducting tunnel junctions. Josephson effects have also been observed in carbon nanotubes [8]. Josephson-type dynamics are applicable to other superfluids. Bose-Einstein condensates also exhibit this type of behavior and this has been studied [9],[10]. Josephson junctions can also be used to study anisotropy in the superconducting energy gap, and it has been used to study the energy gap of lead [11].

MIT Lincoln Laboratory has a continuing effort to fabricate and test Josephson junctions and other superconducting circuit elements. This is contained in a push towards quantum computing and has collaboration with the Orlando group in MIT's Research Laboratory of Electronics. Research within this collaboration has a broad scope and encompasses many facets of superconductive electronics [6, 12, 13, 14].

Making devices with reliable properties requires the accurate characterization and analysis of Josephson junctions. This requires cryogenic testing and analysis of many junctions. The aim of this thesis is the characterization and analysis of Josephson junctions. It encompasses the apparatus for taking data at 4.2 K, the methods for characterizing junctions, the analysis of aggregate data, and finally the progress towards constructing a separate apparatus for testing these circuit elements at 300 mK.

1.2 Superconductivity

Before analyzing superconducting tunneling junctions, it is natural to begin with an overview of superconductivity. Unless otherwise cited, this background is borrowed from references [2] and [15]. Certain materials will exhibit characteristics of superconductivity when it is cooled below a critical temperature T_c that is dependant on the material. Below this temperature electrons will pair together to form Cooper pairs, which behave as bosons. These pairs form a many particle wave function which has phase coherence over macroscopic distances. Each electron of a Cooper pair exists at

an energy below the Fermi surface of $\Delta(T)$. This is known as the superconducting energy gap and it is a temperature dependant property of the material.

Superconductivity was originally described by the London equations:

$$\vec{E} = \frac{\delta}{\delta t}\left(\frac{4\pi\lambda_{\mathrm{L}}^2}{c^2}\vec{J}_{\mathrm{s}}\right) \tag{1.1}$$

and

$$\vec{B} = -\vec{\nabla} \times \left(\frac{4\pi\lambda_{\mathrm{L}}^2}{c}\vec{J}_{\mathrm{s}}\right). \tag{1.2}$$

λ_{L} is known as the London penetration depth; it is a temperature dependant property of the material and will be discussed later. Equation (1.2) can be combined with the Maxwell equation for curl of a magnetic field to yield the second order-equation,

$$\nabla^2\vec{B} = \frac{\vec{B}}{\lambda_{\mathrm{L}}^2}. \tag{1.3}$$

Superconductive materials exhibit two important characteristics that follow from the London equations. Like perfect conductors, they have no resistance (perfect conductivity). This follows from equation (1.1). Resistance is related to the proportionality in Ohm's law of electric field to velocity. In superconductivity, the electric field is proportional to acceleration, which implies there is no limit to conductivity. Equation (1.3) describes the Meissner effect, the property that superconductors expel magnetic fields with a penetration depth of λ_{L}. The Meissner effect is a characteristic of superconductors that perfect conductors do not share.

The London equations may be derived from the quantum mechanical definition of canonical momentum, $\vec{p} = m\vec{v} + \frac{e\vec{A}}{c}$. The argument follows from the assumption that there exists a ground state with zero momentum. This leads to an equation for average velocity,

$$\langle\vec{v_{\mathrm{s}}}\rangle = -\frac{e\vec{A}}{mc}. \tag{1.4}$$

Using n_{s} as the number density of the electrons participating in this state, this leads

to a description of the current density,

$$\vec{J_s} = n_s e \langle \vec{v_s} \rangle = -\frac{n_s e^2 \vec{A}}{mc} \tag{1.5}$$

Defining $\lambda_L^2 = \frac{c^2 m}{4\pi n_s e^2}$, the two London equations follow from taking either the curl or time derivative of equation (1.5). The particles described by these equations are Cooper pairs, with values of mass and charge that are twice that of an electron.

We may write a many-body wave function to describe electron density in a superconductive solid. In a general form, this can be written in terms of magnitude and phase,

$$\Psi(\vec{r}) = |\Psi(\vec{r})| e^{i\theta(\vec{r})}. \tag{1.6}$$

To fulfill the normalization condition, it is required that $\Psi\Psi^* = n_s(\vec{r})$. This requirement allows us to write the wave function in terms of local density of electrons participating in the superconducting state.

$$\Psi(\vec{r}) = \sqrt{n_s(\vec{r})} e^{i\theta(\vec{r})} \tag{1.7}$$

These equations also produce a characteristic length that gives a measure for how deep magnetic fields can penetrate the superconductor. The expression for the London penetration depth is,

$$\lambda_L = \left(\frac{m^*}{\mu_0 e^{*2} n_s^*} \right)^{1/2}. \tag{1.8}$$

The microscopic effects that produced these effects were described by Bardeen, Cooper, and Schrieffer in their 1957 paper which describes BCS theory [16]. BCS theory validated previous research by providing a microscopic mechanism for superconductivity. The interaction that creates the lower energy state of Cooper pairs is a weak electron-phonon interaction. The bound particles interact on distances of order ξ_0.

$$\xi_0 = a \frac{\hbar v_F}{k T_c} \tag{1.9}$$

where a is a constant of order unity and v_F is the fermi velocity, $v_F = \left(\frac{\hbar}{m}\right) \left(\frac{3\pi^2 N}{V}\right)^{1/2}$

[17]. The result from BCS theory most pertinent to this research is the definition of the energy gap. The zero-temperature value for Δ is given by,

$$2\Delta(0) = 3.52 k_{\mathrm{B}} T_{\mathrm{c}}. \tag{1.10}$$

Δ has very little variation up to $\frac{T_{\mathrm{c}}}{2}$. Close to T_{c} it has behavior given by,

$$\Delta(T) \approx 3.2 k_{\mathrm{B}} T_{\mathrm{c}} (1 - \frac{T}{T_{\mathrm{c}}})^{1/2}. \tag{1.11}$$

1.3 The Josephson Equations

The derivation of the equations that govern Josephson tunnel junctions comes from describing Cooper-pair tunneling as coupled wave functions across the barrier. We consider the time dependant Schrödinger equation for the wave functions on both sides of the insulating gap [18],

$$\begin{aligned} i\hbar \frac{\delta \Psi_1}{\delta t} &= U_1 \Psi_1 + K \Psi_2 \\ i\hbar \frac{\delta \Psi_2}{\delta t} &= U_2 \Psi_2 + K \Psi_1 \end{aligned} \tag{1.12}$$

where K is a coupling constant, and $U_{1,2}$ are the energies of the wave functions. The only relevant energy is the energy difference between the sides. With a voltage source V present, the energy difference becomes $U_2 - U_1 = e^* V$ where e^* is the effective charge, twice the charge of an electron. These substitutions lead to the new equations,

$$\begin{aligned} i\hbar \frac{\delta \Psi_1}{\delta t} &= -\frac{e^* V}{2} \Psi_1 + K \Psi_2 \\ i\hbar \frac{\delta \Psi_2}{\delta t} &= \frac{e^* V}{2} \Psi_2 + K \Psi_1 \end{aligned} \tag{1.13}$$

Combining equation (1.13) with the ensemble wave function expression in equation (1.7) introduces pair density into these equations. Evaluating the imaginary part

yields a relationship for change in carrier density,

$$\frac{\delta n_{s1}}{\delta t} = \frac{2}{\hbar} K (n_{s1} n_{s2})^{1/2} \sin\phi = -\frac{\delta n_{s2}}{\delta t} \tag{1.14}$$

The phase difference ϕ is defined as $\theta_2 - \theta_1$. This relationship can be turned into a definition of current by defining l, the tunnel junction barrier width, and can be further simplified with the assumption that the pair densities are equal, which must be true because change in carrier density would lead to charge imbalance between the electrons and ions. This carrier density is maintained by the circuit connected to the junction [15].

$$J = l e n_s \frac{\delta n_s}{\delta t} = \frac{2eKn_s^2 l}{\hbar} \sin\phi = J_c \sin\phi \tag{1.15}$$

This is known as the Josephson current-phase relation. While this is not a derivation of J_c, as K is an assumed quantity, it does follow the correct limits, e.g., if the coupling is removed, $K = 0$, then J_c disappears and there is no tunneling. A derivation of the critical current was done by Ambegaokar and Baratoff and is based in microscopic theory [19]. It was later verified experimentally by Milan Fiske [20]. The result pertinent to this thesis is the expression for J_c in terms of area A and normal resistance R_n,

$$J_c = \frac{1}{R_n A} \left(\frac{\pi \Delta(T)}{2e} \right) \tanh \left[\frac{\Delta(T)}{2k_B T} \right] \tag{1.16}$$

To continue the macroscopic derivation, substituting equation (1.7) into equation (1.13) and looking at the real component yields expressions for change in phase,

$$\begin{aligned} \frac{\delta\theta_1}{\delta t} &= -\frac{K}{\hbar} \left(\frac{n_{s2}}{n_{s1}} \right)^{1/2} \cos\phi + \frac{e^* V}{2\hbar} \\ \frac{\delta\theta_2}{\delta t} &= -\frac{K}{\hbar} \left(\frac{n_{s1}}{n_{s2}} \right)^{1/2} \cos\phi - \frac{e^* V}{2\hbar} \end{aligned} \tag{1.17}$$

With the continued assumption that $n_{s1} = n_{s2}$, the difference of these equations

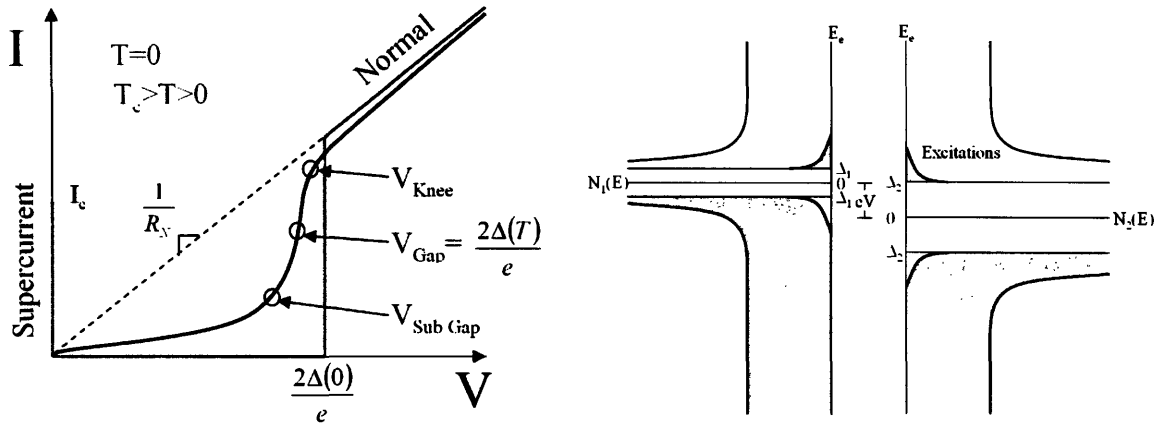

Figure 1-1: (Left) Sample I-V traces of a Josephson junction at different temperatures with features relevant to analysis labeled. The blue curve corresponds to $T = 0$ K and the red curve corresponds $T_c > T > 0$. (Right) Energy diagram of a Josephson junction with applied voltage V. Thermal excitations have put some electrons in the quasiparticle regime. For as long as there can be supercurrent, as governed by equation (1.16), there is no voltage gap. As soon as the applied current exceeds J_c, voltage between the two superconductors jumps up until the superconducting band of one is level with the normal band of the other. This allows for quasiparticle tunneling. This persists even when the voltage is then reduced, because there are still electrons excited that will continue to tunnel resulting in a subgap voltage.

simplifies to the other Josephson junction equation, the voltage-phase relation:

$$\frac{\delta\phi}{\delta t} = \frac{2eV}{\hbar} \tag{1.18}$$

where V is the voltage across the junction. An alternate derivation of these equations is given in reference [21].

A sample current-voltage diagram of a Josephson junction is shown in figure (1−1). The diagram extends symmetrically into the negative $|V|$ and I domain, but is not shown for simplicity. The junction is hysteretic, not returning to the supercurrent from $V > 0$ until arriving at $V = 0$ through the subgap regime. This is explained in the energy diagram shown in figure $(1 - 1)$.

The slope of the normal regime is known as the normal conductance, which follows the temperature dependance of normal-electron tunneling, but is nominally the same at cryogenic temperatures or room temperature. The energy gap is directly related to the point at which the normal regime ends and subgap regime begins. At nonzero

temperatures below T_c, this point is compressed in V due to the effects of decreasing Δ, and the reduction is thermally spread. For analysis, the voltage at which the normal regime ends is labeled V_{knee} and the voltage at which the subgap regime ends is labeled V_{subgap}. The voltage that corresponds to the energy gap is between these and is denoted V_{gap}.

1.4 Relation of Shape to Critical Current

The simplest way to calculate the critical current of a junction is to assume that the critical current density is spatially invariant along the junction barrier. Two relationships, equation (1.15) and equation (1.16), define conditions for this assumption. The first, that ϕ is constant, will be addressed in section (1.5). The second assumption is based on the geometry and composition of the junction. Holding Δ and T as constant is reasonable in the case of a junction of uniform composition, which is the case treated here. J_c is proportional to conductance, which is exponentially dependant on barrier thickness. This is predicted by the WKB approximation describing tunneling when applied to barriers of uniform potential [18]. For a barrier that has current density J_0 at thickness t, this relationship can be given by,

$$J_c = J_0 e^{\frac{t-d}{t}}, \tag{1.19}$$

where d is the thickness of the junction. Two geometries are of particular interest. The first is trivial, a circular barrier of diameter δ and uniform thickness t. The critical current of this geometry is,

$$I_c = \pi J_0 \frac{\delta^2}{4}. \tag{1.20}$$

The other geometry is picked for its relevance to likely fabrication features in Josephson junctions. The barrier is a uniform disc of thickness t with a thicker ring of insulator around the edge. This edge has additional thickness t_0 and width d_0. This

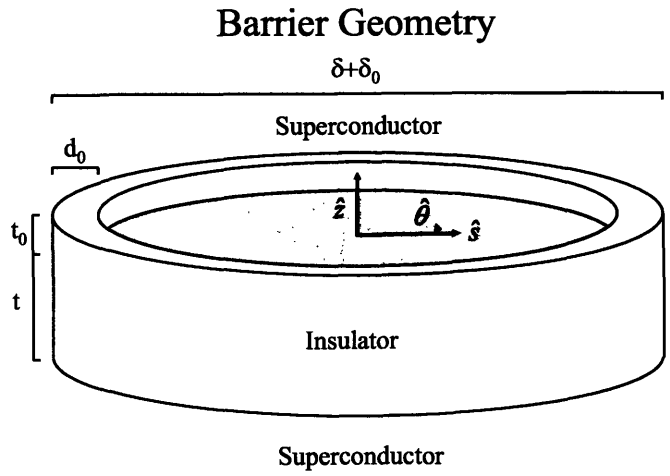

Figure 1-2: Diagram of the Josephson junction barrier model being analyzed. This analysis is most convenient in cylindrical coordinates.

geometry can be seen in figure $(1-2)$ and is given by,

$$\begin{aligned} d = t \quad &: \quad \leq s \leq \frac{\delta}{2} - d_0 \\ d = t + t_0 \quad &: \quad \frac{\delta}{2} - d_0 \leq s \leq \frac{d}{2} \end{aligned}$$

The integral to determine $I_c(\delta) = \int J_c(\delta) dA$ simplifies to,

$$I_c = \delta^2 \frac{\pi J_0}{4} - \delta d_0 \pi J_0 \left(1 - e^{-\frac{t_0}{t}}\right) + d_0^2 \pi J_0 \left(1 - e^{-\frac{t_0}{t}}\right). \tag{1.21}$$

This definition has a linear dependence as well as a constant term, rather than the simple quadratic prediction. If $t_0 \gg t$ such that the exponential term is essentially 0, the equation reduces to the expected I_c of simple disc junction with a reduced diameter $\delta - d_0$.

1.5 Self-Limiting Induction Effects

Just as superconductors can have their superconductivity quenched by a magnetic field, Josephson junctions too can have their critical current modified by a magnetic field. The relation of magnetic field to critical current is given by [2],

$$I_c(\Phi) = I_c(0)\left|\frac{\sin(\pi\Phi/\Phi_0)}{(\pi\Phi/\Phi_0)}\right| \tag{1.22}$$

where $\Phi_0 = \frac{h}{2e}$ is the flux quantum. Because currents are flowing across the barrier of a junction, this induces a magnetic field. These fields affect the phase difference between the sides of the junction and therefore change the critical current. This is demonstrated in [2] and [22] for a rectangular junction and very extensively treated in [23] for a square junction. Of particular interest to this thesis is examining this effect for circular junctions. A useful constant in this examination is known as the Josephson penetration depth,

$$\lambda_J^2 = \frac{\hbar}{2eJ_c\mu}\frac{1}{(2\lambda_L + d)}, \tag{1.23}$$

where λ_L is the London penetration depth as defined in equation (1.8) and d is the barrier thickness. The London penetration depth of niobium is 39 nm and barrier distance is of the order of 1 nm. The target J_c is about 5 $\frac{\mu A}{\mu m^2}$. A typical λ_J with these parameters is about 25 μm.

This effect is explored through simulation. We define a circular junction in cylindrical coordinates with its axis aligned with the $\hat{z}$ axis and with a radius r. it can be assumed that the current is only is only axial and only depends on radius, $\vec{J} = J(s)\hat{z}$. The gradient of the phase is given by [22],

$$\vec{\nabla}\phi = \left(\frac{1}{J_c\mu\lambda_J^2}\right)(\vec{B} \times \hat{n}) \tag{1.24}$$

where $\hat{n}$ is the normal vector that points axially from the first to the second superconductor, and $\vec{B}$ is the self-induced magnetic field. The self-induced magnetic field

is must only have a component in the $\hat{\theta}$ direction that depends only on s. A radial magnetic field would either have to break symmetries in the problem or violate $vecbigtriangledown \cdot \vec{B} = 0$, and an axial field would be parallel to current. Ampere's law may be used to relate the magnetic field to current, $\vec{\nabla} \times \vec{B} = \vec{J}\mu_0$ [18]. The limited components of current and magnetic field simply the problem. Application of equation (1.15) allows the extraction of a first-order differential equation that relates phase and magnetic field. Another first-order differential equation can be extracted from equation (1.24),

$$\frac{\delta\phi}{\delta s} = \frac{1}{J_c \mu \lambda_J^2} B_\phi(s), \tag{1.25}$$

$$\frac{\delta}{\delta s}\left(sB_\phi(s)\right) = s\mu J_c \sin\phi. \tag{1.26}$$

Solving equation (1.25) for $B_\phi(s)$ and plugging it into equation (1.26) yields the second-order differential equation, which can simplified with the dimensionless variable $l = \frac{s}{\lambda_J}$,

$$\frac{\delta^2\phi}{\delta l^2} + \frac{1}{l}\frac{\delta\phi}{\delta l} = \sin\phi \tag{1.27}$$

The total current of the junction is given by,

$$I_c = 2\pi J_c \lambda_J^2 \int_0^{\frac{r}{\lambda_J}} \sin(\phi) l \, dl \tag{1.28}$$

This integral may be evaluated numerically. Values for $\frac{\delta\phi}{\delta l}$ may be evaluated from equation (1.25) in which B_θ is known because of Ampere's law and the calculated enclosed current. Combining these with equation (1.27) allows for a second order Taylor expansion of $\phi(l)$. Finding an initial value for ϕ is not trivial, however. Trial and error is necessary to set value of ϕ at the origin to whatever value will maximize the current, giving a true maximum of I_c. This value is found by sweeping $\phi_{s=0}$. The best value starts at $\frac{\pi}{2}$ in small junctions and approaches 0 as the size increases. This value is plotted in figure $(1-3)$ along with a plot of maximum current vs. junction radius. In the dimensionless units of this analysis, the unbiased curve is $\frac{I_c}{J_c\lambda_J^2} = \pi\left(\frac{r}{\lambda_J}\right)^2$. It is clear from the graph that junctions less than 2 λ_J in radius have

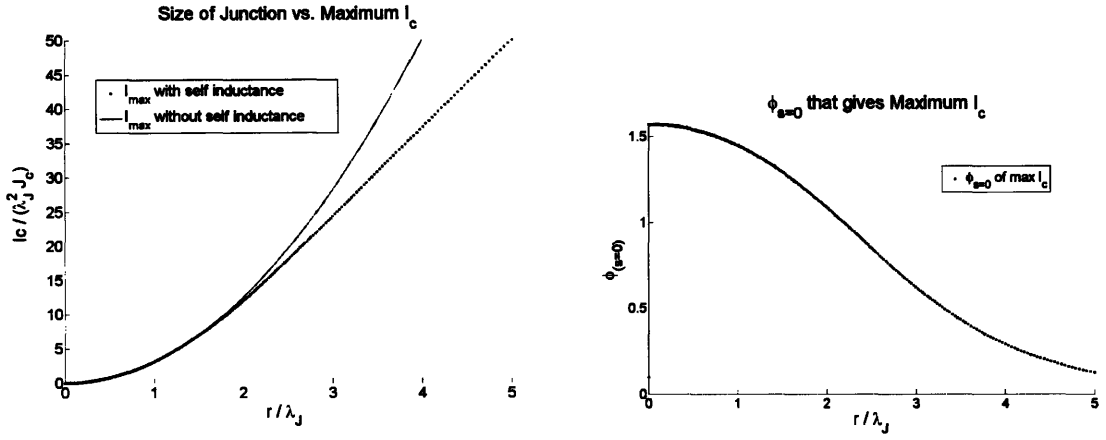

Figure 1-3: (Left) Dimensionless plot of maximum current against Josephson junction radius. The two lines are indistinguishable until nearly $2\lambda_J$.(Right) Calculated starting value of ϕ used at $s = 0$ to give the maximum value of I_c. The curve originating at $\frac{\pi}{4}$ is expected because in small junctions the self field doesn't have a big effect so the current can be maximum everywhere. As the size increases the starting value goes to 0, which means the current is concentrated at the edge.

negligible deviation from the unbiased graph. We may safely ignore this effect in our analysis of junctions with $r < \lambda_J$. These results are consistent with with results in [2],[22] and [23]. The code used to simulate this effect is shown with comments in addendum ($B.1$).

Chapter 2

^{4}He Josephson Junction Characterization

2.1 The Junctions

The 4.2 K ^{4}He initiative is designed to test niobium trilayer Josephson junctions below the critical temperature of Niobium, 9.26 K. Niobium is a good choice for a superconductor because of its high critical temperature and depth of research regarding its material properties [25, 26]. The devices are fabricated onto six inch diameter wafers. Each wafer contains 25 complete reticles, each of which is called a die. These are labeled by a letter (column) and a number (row). In each die is an identical set of chips. My testing focuses on a chip with 6 Josephson junctions. An example of such a test structure is shown in figure $(A-1)$.

The junctions are fabricated at Lincoln Laboratory in connection with the Low Temperature Superconducting Electronics (LTSE) and Deep Submicron (DSM) projects. A cross section of the junctions is shown in figure $(2-1)$. The junction is formed by separating a layer of superconducting niobium from a circular niobium pillar with an insulator, 1 nm of amorphous aluminum oxide. In addition to the oxide barrier, $6-7$ nm of aluminum is left from processing. Aluminum is a normal metal at this temperature. Because the metal is so thin, the junction can still be treated as a Superconductor Insulator Superconductor (SIS) junction due to the proximity effect

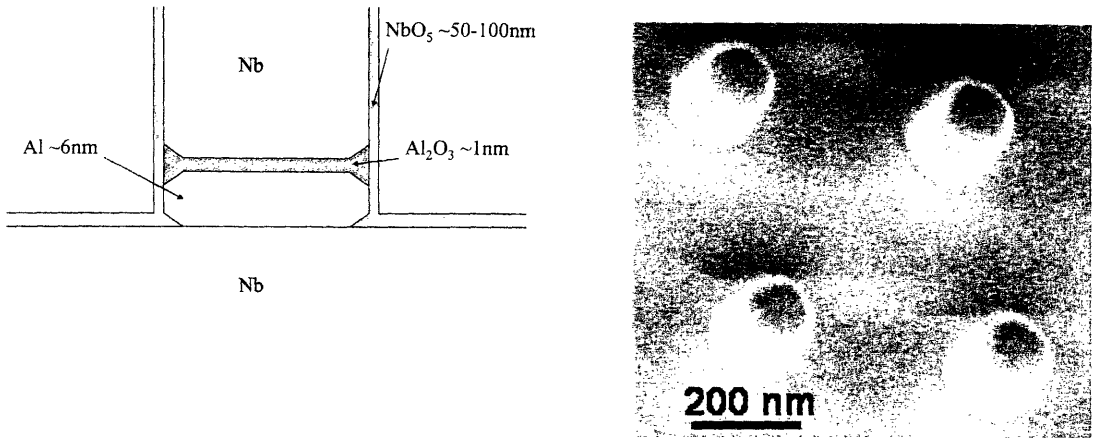

Figure 2-1: (Left) This diagram shows the materials that make up a Josephson Junction in the Niobium trilayer junctions. The diagram is not to scale. (Right) A scanning electron microscope image of the pillars that will form Josephson Junctions. These are very small junctions, approximately 0.2 μm in diameter.

from the superconducting niobium [2]. The resistance of the barrier in quasiparticle tunneling dominates that of the aluminum layer, so its addition to R_n is negligible. A Scanning Electron Microscope (SEM) image of four junctions is shown in figure $(2-1)$, SEM imaging is used as part of the fabrication feedback process.

A 1-nm oxide barrier means that there are only three to four monolayers of insulator between the niobium and the aluminum. As shown in the diagram, it is likely that there are oxidation effects that pollute both the niobium and the aluminum. These increase the barrier thickness along the perimeter of the junction. There are other fabrication faults but most of them drastically modify the behavior of the junction, making them distinguishable. For example, resistive channels can form directly through the barrier and give the appearance of leaky or shunted junctions.

One of the most critical details that can be extracted from cryogenic data is information about junction size. The electrical diameter of the junction can be broken down into several terms,

$$d_{\text{electrical}} = d_{\text{drawn}} + d_{\text{optical}} + d_{\text{NbOx}} + d_{\text{unknown}}. \tag{2.1}$$

$d_{\text{electrical}}$ is the effective diameter of the junction based on electrical characteristics. d_{drawn} is the actual diameter of the junction as specified by the design. All the other terms may be thought of as biases, as they are deviations from the desired size. d_{optical} represents the size change due to optical lithography. This is measured by a SEM, and it has been shown to be size dependent, taking a range of value between 0.03 and 0.15 μm. d_{NbOx} is the size loss due to oxidation. NbO_5 forms along the edge of the junctions with a depth of $50 - 100$ nm. This material is a conductor at room temperature, so its effect cannot be adequately measured without cooling down the chip to 4 K, at which point the NbOx has frozen out. Approximate values can be determined by oxidizing different size wires of Niobium and observing them with a SEM. This has been done, and the results are size independent, taking values $0.1 - 0.2$ μm. d_{unknown} is a term that encompasses deviations from the other biases as well as unknown factors. Because this information is unavailable at room temperature, this is cryogenic testing must be used to determine.

2.2 Apparatus Description

The apparatus used to test Josephson junctions at 4.2 K was being used previously to my involvement in the project. The probe relies on a four-point measurement of devices on a chip dipped into liquid helium inside a vacuum insulated dewar. When submerged in helium, the electronics on the chip are held at a consistent 4.2 K. This temperature is the boiling point of Helium at standard pressure.

An electronic diagram of the ^{4}He apparatus is shown in figure $(2 - 2)$. A voltage is applied across a variable resistor to create a current source. The resistors span each decade from 1 Ω to 100 kΩ to allow for a range of currents. On each side of this source resistor, 880 kΩ resistors are connected to the positive and negative inputs of a differential amplifier. Because the source resistance is known, this voltage provides a measure of current passing through the device. This measurement is displayed as the vertical axis on the oscilloscope.

The source current is brought to the I_+ lead of the switching box on top of the

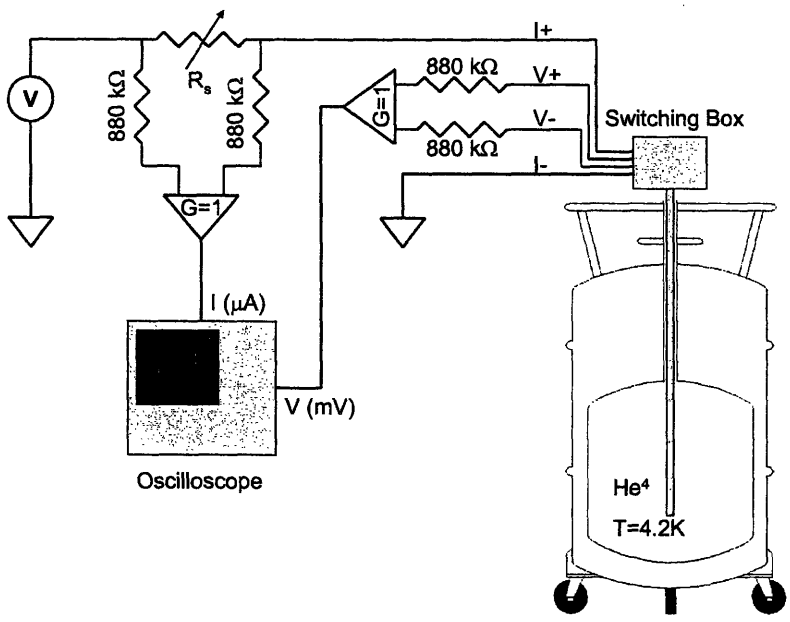

Figure 2-2: 4.2 K Peterson testing apparatus. The oscilloscope is connected to a computer that is used to control readout and record the data.

Peterson probe. This is a long probe that sticks into the helium dewar. The probe has a switching box on top with four BNC inputs for $V_{\pm}$ and $I_{\pm}$. There are twenty four switches in addition to four grounding and shorting switches to connect these inputs to the cables that lead down to the chip. Shorting and grounding allows discharge of built up voltage that would otherwise damage the chip. This is called the make-before-break connection method which entails connecting to the device before breaking the connection across the device.

The chip is held by a spring-and-screw mechanism which holds the chip against a set of gold leads that maintain electrical contact. This allows for reliable contact and quick changing of chips. Each chip is has 24 contact pads and 24 grounding pads.

Voltage is measured across the $V_{\pm}$ leads that connect on separate paths directly next to the junction. This minimizes the effect of the large source current creating line resistance across $V_{\pm}$. The $V_{\pm}$ leads also run through 880 kΩ resistors and into a differential amplifier with 100 MΩ input impedance. This voltage is the device voltage. Finally the I_{-} channel is connected to common ground.

The oscilloscope is connected to a computer which has been fitted with custom data collection software. This software was written by George Fitch, and it communicates with the analog oscilloscope and controls collection times. The data is acquired by averaging the current measurements acquired by sweeping the voltage across the region of interest. The data then undergoes preliminary analysis, and is and saved for further analysis.

2.3 Characterization of Josephson Junctions

Besides cryogenic testing, one of my main contributions to the group's process testing efforts was to develop and test custom software in MatLab that can be used to analyze current-voltage traces of devices. The algorithm to analyze current-voltage traces is shown in addendum ($B.2$). The software also has methods to analyze aggregate statistics of wafers and entire runs. The user controls the program by way of an user interface shown in figure ($A-2$). The GUI is important, because this program will

likely be used to analyze data after my involvement in the project, so it needs to be easy to use.

The data is read from a *ASCII .txt* file, which has been labeled with a scheme that reveals everything about where the data comes from. The scheme is, Group,Year_Run Number_Wafer_Die_Mask_Reticle_C_ascii.txt. for example,

$$LTSE04\_14\_1\_B4\_PT6\_11\_C\_ascii.txt$$

is the 14th LTSE run in 2004, wafer 1, from the $B4$ Die and 11th chip on the $PT6$ mask. The data is put into tab delimited columns. The first column is the voltage read directly from the scope in mV. Each trace is made up of two additional columns. The second column is the only relevant one, the first is a zoomed in version of the middle of the trace. The second column is the value of the junction current in μA. It requires the input of the source resistor, which is done by the program initially used to record the data.

The first step in the software is to read in the data from these files. The raw data is grouped with information about the chip by looking at the filename. This information is then compared to a local database of masks to find out what devices are expected to be in each location. The program is fit to deal with junctions, strings of junctions, resistors, or vias. Strings of junctions exhibit the same behavior as single junctions except the trace is broadened in the voltage domain proportionally to the number of junctions in the string.

At this point the data is passed to a subroutine that analyzes all data the same way. The first step is to remove excess points from the data. When the original data is saved, it includes values up to the maximum voltage of the oscilloscope, which might be clipped. The final observed value is reported as every uncollected data point. These values are removed before analysis.

The characterization begins with testing for known failure types, e.g., null data, open and short circuits. Null data sets contain no data after removing the excess points. An open circuit doesn't allow any current through at any voltage, which is

checked for by fitting the data to a horizontal line. This indicates a gap in the circuit, not always associated with the junction. A short circuit never has voltage across it when current is applied, this is evident when the trace is very small in the voltage regime. This is the trace expected for a superconducting via.

The next step in the analysis process is to find the knee voltage. Niobium's value of $2e\Delta$ is close to 3 mV, therefore, It looks for the knee at 3 mV times the number of junctions in the string. Once the knee voltage is identified, the algorithm looks at higher voltages for the normal regime. This regime is identified by similarity of slope and extends from above the knee to the edge of the trace. This region will be used to find normal resistance.

The algorithm also looks for a subgap regime around 0.75 mV times the number of junctions in the string. Once this region has been identified by similarities in slope, it averages slope to determine the subgap resistance. The averaging algorithm on the oscilloscope sometimes averages poorly, leaving half the points obviously on a higher line and half on a lower line. This would create a large problem in curve fitting if not corrected. The algorithm is designed to correct for this: the trace is defined as "noisy" if the points fall close to two different current values throughout the length of the sub gap regime. The current value with more points is considered correct and the other is shifted by an amount to equilibrate their means. This allows for more accurate fitting of the subgap. This is shown in figure $(2-3)$.

The normal resistance is calculated by applying a least squares linear fitting algorithm to the normal regimes on both sides of the axis. Using both sides of the axis eliminates potential voltage offsets. The line is expected to go through the origin, as it is Ohm's law. With both quadrants present, it is safe to allow for a nonzero current intercept and justify it as an offset in current or voltage.

The program is less reliable for determining subgap resistance. This is because the data in this region does not always appear linear, and we do not have high resolution in this region. The individual subgap resistances for each side are calculated and averaged to provide this value. At this point, the subgap and normal resistances are compared. If they are similar, then the device is assumed to be resistive and a linear

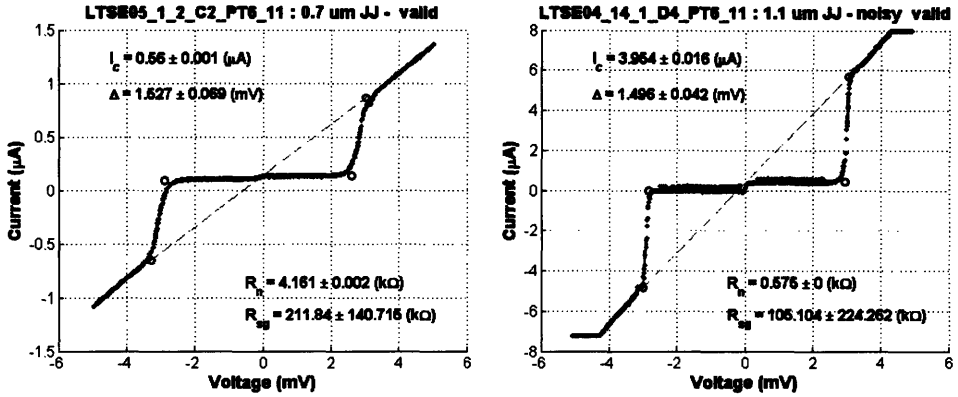

Figure 2-3: Current voltages traces of two working junctions. These are direct output plots of the program. The second shows two artifacts of the data collection method. The presence of two distinct lines in the sub gap regime is because of the averaging, and the slight jump close to the negative knee is a mistake that comes from stopping data collection while the current is still sweeping back and forth.

fit is made to the whole set of data.

This is also the part of the routine where leaky and shunted junctions are identified. Examples of these two failure modes are shown in figure $(A-3)$. Shunted junctions are identified because of the voltage jump at the origin. Leaky junctions are determined in two ways: either a similarity in subgap resistance to normal resistance but with overall resistance nonlinearity, or if the knees aren't steep enough.

To determine the characteristic voltages and currents of the junction, the program uses a series of linear fits. It estimates a slope for the knee and fits a line to the knee section. The intersection of this line and the normal line is at the knee voltage. The intersection of this line and the subgap line provides the subgap voltage. Averaging the positive and negative voltage measurements for each of these eliminates the offset. The algorithm assumes an error in measurement associated with scope resolution that is the distance in current between the closest points. The parameters extracted from each working trace are V_{knee}, V_{subgap}, and R_n.

2.4 Analysis of Wafers

Analyzing individual traces for characteristics is very important but the most useful feedback cryogenic testing provides is from analyzing wafers as aggregates of junctions. Fabrication parameters are varied from wafer to wafer, so comparing wafer statistics is the most enlightening.

The two types of devices that are useful to analyze are resistors and Josephson junctions. While resistor analysis is full of subtly, it is not the focus of this thesis and so not much detail will be paid to it. In brief, resistor analysis is centered on the measured resistance and expected resistor width. Only one dimension is varied so a linear fit can be used to determine trends in width as well as resistivity. This analysis is based on the definition of resistance as $R = \frac{\rho l}{A}$ where resistivity ρ and length l are constant for all devices. Area A is allowed to vary across devices. The equation to fit to is

$$\frac{W}{R_{\mathrm{s}}} + \frac{W_0}{R_{\mathrm{s}}} = \frac{l}{R_{\mathrm{n}}}, \tag{2.2}$$

with l being the length of the resistor, 100 μm. R_{n} is the measured normal resistance, W is the drawn size, W_0 is the sum of all biases and R_{s} is the sheet resistance, a constant that only depends on the resistivity and height of the junction. A least-squares fit will give the best values of W_0 and R_{s}. This analysis is done by die, and plotted by location on the wafer.

The analysis of Josephson junctions is covered in great depth in Chapter (3). The program automatically performs the analysis to determine parameters that are of use to fabrication. The parameters that are calculated for each die are the critical current density J_{c} and average process bias d_0. These results are plotted on displays of the wafers such as figure $(A-4)$.

The program also plots median characteristic values for each wafer. For Josephson junctions, it plots J_{c} and δ_0, and for resistors, it plots R_{s} and W_0. An example is shown in figure $(A-5)$. A final summary that this program provides is of device type. This breaks down by size and wafer number how many of each failure mode there were. An example of this plot is shown in figure $(A-6)$.

Chapter 3

^{4}He Cryogenic Results

3.1 Energy Gap Determination

The most valuable asset of 4.2 K cryogenic testing at is the rapid feedback of otherwise unattainable information. Room-temperature testing can provide a value for normal resistance, but this resistance cannot be separated from the NbOx conductor on the outside of the junction. Likewise J_c can be measured at room temperature to within 10%, but information about the size of the junction cannot be determined unless it is cooled. Additionally, whether or not the junction functions correctly is also unattainable at room temperature.

The junctions are drawn between 0.4 μm and 1.1 μm in diameter, less than 5% of λ_J which is 25 μm. With sizes this small, self-field effects do not significantly impact the critical current, as shown in section (1.5).

The first piece of data calculated is the superconducting energy gap. $2\Delta/e$ is located between V_{subgap} and V_{knee} as seen section (1.3). The average of these voltages is used to calculate the energy gap. Table (3.1) lists the mean values of Δ reported for each run. Histograms of calculated Δ are shown with the superimposed gaussians used for finding the mean and variance are shown in figure $(3-1)$. All analysis follows standard error determination [27].

Experimental values of Δ confirm the assumption of treating this as a superconductor insulator superconductor (SIS) junction. The energy gap of a metal insulator

Run	Valid Junctions	Δ meV
LTSE04_14	106	1.508 ± 0.044
LTSE05_1	189	1.513 ± 0.031
DSM205_19_8	96	1.511 ± 0.020

Table 3.1: Mean values of Δ for three runs. BCS predicted value for niobium is $\Delta_{(T=0)} = 1.40$ meV, from equation (1.10). This has been experimentally shown to be 1.55 meV, which is shown to be constant over $0.4 - 4.2$ K [25].

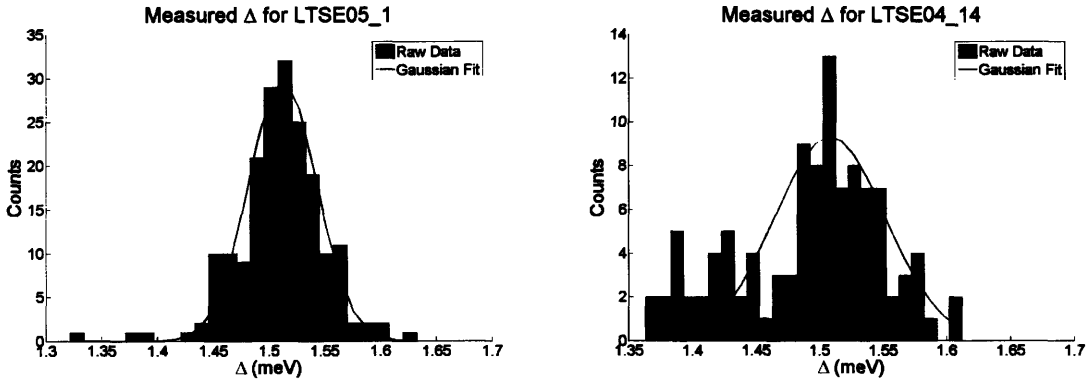

Figure 3-1: Histograms of measured Δ from two of the three runs. The gaussian is only used for purposes of reporting a mean and variance in mean for Δ.

superconductor (NIS) junction is Δ/e, half the gap of an SIS junction [2]. The individual junction's energy gap is used in further calculation. Δ shows no explicit dependance the on size of the junction. This is consistent with the prediction that Δ only depends on temperature and the material parameters. Variations in Δ can be attributed to inhomogeneities in the materials.

The other parameter that is directly taken from the current-voltage trace is the normal resistance. R_n is the inverse of the slope in the normal regime. Together with equation (1.16), I_c can be calculated.

3.2 Critical Current and Process Bias

The junctions are fabricated with an expected J_c and expected diameter. The expected J_c can vary with the wafer, as it is a parameter of fabrication. Any description

of critical current density must include discussion about the geometry of the junction. The diameter of the junction is specified, but shifted by an unknown quantity δ_0, see equation (2.1). Additionally the barrier is not necessarily uniform.

Two steps are taken to simplify this analysis. The first step is the assumption is that the parameters of interest, δ_0 and J_c, do not vary on each chip. Additionally, a model must be adopted for the junction barrier. The simplest model neglects barrier pollution and assumes the barrier to be a flat disc. This is defined by equation (1.20). Bias is accommodated by separating the diameter into δ and δ_0, where δ is the sum of drawn size and δ_{optical}. Values for δ_{Nb0x} have been observed, but since the bias is constant with respect to junction diameter, we may let it vary and determine it for each chip. Therefore, the measured bias is a sum of the niobium oxidation bias and unknown biases which is known as the process bias.

To begin the analysis of bias and critical current density, I_c is written in a form that is quadratic in δ. There is no reason to deal with the quadratic though; the repeated roots imply that it is possible to linearize. The following line can be used to fit the data in this model,

$$\sqrt{\frac{4\,I_c}{\pi}} = \sqrt{J_c}\delta + \sqrt{J_c}\delta_0. \tag{3.1}$$

A least-squares method is used to fit the working junctions from each chip. The algorithm looks for points to throw out that are clearly outliers. It does this by recalculating the fit as is a given point had not been there. If removing a point changes the fit a great deal and would leave at least two points to fit, it removes the point from the fit. This allows the program to discount anomalies of the junction fitting algorithm. An example of a set of fitted data is shown in figure $(A-7)$.

There are several ways to organize the data to make viewing trends obvious. The most useful is to plot the desired data on top of the wafer so trends across the wafer can be seen. This is known as a wafer map, and an example can be seen in figure $(A-8)$. Another way of organizing the data is to show it as a comparison across wafers of the same run. An example of this is shown in figure $(A-5)$.

The results of this analysis reveals two important things: typical values of parameters and trends across wafers and runs. Values from this analysis show high variance inside both wafers and runs. Variance between wafers in the same run is expected because processing is intentionally different. Variance inside single wafers can be attributed to processing inhomogeneities as well as inaccuracies associated with fitting lines to between 2 and 6 points.

Looking at the wafer maps, it becomes obvious that the assumption that these parameters change across wafers is valid. The effects of stresses and strains during deposition and processing (etching) make the junction parameters vary. Looking at figure $(A-8)$, the top left of the wafer has low process bias and low critical current while the bottom left has the opposite. In general, areas with low bias were observed to have low critical current density.

Values for process bias range from enlargements less than 0.1 μm to reductions less than 0.6 μm. The expected diameter pollution of niobium oxide falls into this range because it is between 0.1 and 0.2 μm. Enlargements and reductions greater than 0.4 μm are not physical. The smallest junction is 0.43 μm, so a bias of that order would completely close off these junctions. Junctions of this size did yield on chips with calculated diameter reductions greater than 0.5 μm. Similarly, enlargements would imply that there is no oxidation or that the junction has somehow expanded its effective area past what was drawn. Observation of oxidation makes these results nonphysical as well.

Similar conclusions may be drawn from J_c. The majority of wafers analyzed have a target J_c of 5 $(\frac{\mu A}{\mu m^2})$. Critical currents were consistently calculated to be lower than this target. This means that either the fitting is done poorly, or the resistivity is increased by a thicker barrier than anticipated. J_c is best evaluated on a wafer by wafer basis because of the varying target Jc. In the case of wafers with target J_c of 5 $(\frac{\mu A}{\mu m^2})$, a histogram and gaussian fit current by die is shown in figure $(3-2)$. Typical values based on the gaussian fits are tabulated in table (3.2).

Variable	Typical Value
J_c	$4.88 \pm 2.81 \left(\frac{\mu A}{\mu m^2}\right)$
δ_0	-0.35 ± 0.12 (μm)

Table 3.2: Typical values of fitting parameters from the linear model. For finding J_c, only junctions with expected J_c of 5 $\frac{\mu A}{\mu m^2}$ are used. For finding δ_0 all junctions are used.

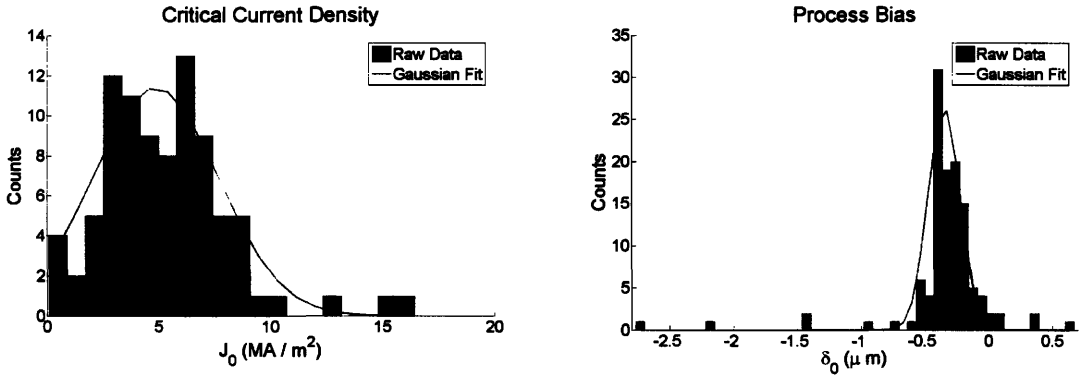

Figure 3-2: (Left) Histogram and Gaussian fit of fitted die J_c from die of wafers with expected J_c of 5 $\frac{\mu A}{\mu m^2}$. The gaussian is used for mean and error determination with results listed in table (3.2). (Right) Histogram and gaussian fit of the process bias of all die analyzed. The gaussian is used for mean and error determination with results in table (3.2).

3.3 Barrier Pollution Analysis

Knowing that fabrication never produces ideal junctions, it is natural to question the validity of such an ideal barrier model. One way inaccuracies would manifest would be reoccurring nonlinearities in the data. A way to check for this is to analyze the residuals of the linear fit. If certain diameters consistently deviate in the same way, it indicates the necessity of a new model. This could also mean that new values are needed for expected biases. Fitting residuals from run LTSE05_1 are shown in figure $(A-9)$. The residuals plotted on this graph exhibit a clear size dependance, indicating a systematic problem with analysis.

Another check of the model is executed by relaxing the linear assumption and fitting the data to a quadratic. If this model is accurate, the determinant of the fitted

Variable	Simple Model	Perimeter Pollution
a	$\frac{\pi J_0}{4}$	$\frac{\pi J_0}{4}$
b	$\frac{\delta_0 \pi J_0}{2}$	$\frac{\delta_0 \pi J_0}{2}\left[1-2\frac{d_0}{\delta_0}\left(1-e^{-\frac{t_0}{t}}\right)\right]$
c	$\frac{\delta_0^2 \pi J_0}{4}$	$\frac{\delta_0^2 \pi J_0}{4}\left[1-4\frac{d_0}{\delta_0}\left(1-e^{-\frac{t_0}{t}}\right)+4\frac{d_0^2}{\delta_0^2}\left(1-e^{-\frac{t_0}{t}}\right)\right]$

Table 3.3: Table of fit values for the quadratic fit $y = ax^2 + bx + c$ of $I_c(\delta)$.

quadratic would be zero, indicating repeated roots. Before performing this check, it is useful to speculate what the determinant should be in an alternate model.

A natural model to adopt is one that treats perimeter pollution effects in a simple way. The model in equation (1.21) and figure (1−2) treats this effect. We must again add the bias effect, so δ becomes $\delta + \delta_0$. Because the barrier is only a few monolayers in thickness, it is likely that the pollution would also only be a few monolayers in thickness. If the barrier were much thicker, that section of barrier would probably be too thick to contribute significantly to the critical current. This model does assume, however, that the pollution is uniform thickness and has width and height that is independent of size. For this reason a model like this will merely serve to give a bound for this effect rather than produce actual numbers. While the quadratic fit may be used in either model, the parameters represent different values. The parameters of the $y = ax^2 + bx + c$ fit are shown in table (3.3) in terms of the constants of the models.

The perimeter pollution model changes the linear and constant term of the fit. A way to compare the models quantitatively is by looking at $b^2 - 4ac$. For the simple model this is 0 because the roots are repeated. For the pollution model this is not zero. Dividing by a^2 reduces it to parameters of the pollution,

$$\frac{b^2 - 4ac}{a^2} = -16\, d_0^2 \left(1 - e^{-\frac{t_0}{t}}\right) e^{-\frac{t_0}{t}}. \tag{3.2}$$

Because fitting to a parabola requires at least 3 points, the data available to this analysis is very small. Also, in sets with small numbers of data points, bad points can throw off the fit a great deal. A histogram of this modified determinant shows

77 of the 81 points clustered together at the origin and the last 4 are discarded as outliers. A gaussian fit to the histogram is shown in figure $(A-10)$. The result does not fit either model perfectly. There is a great deal of deviation from the origin, unlike the simple model predicts, and while the pollution model predicts a negative mean, the determinant is centered around the origin.

This data may be used to predict a maximum value for the perimeter pollution depth, however. Assuming t_0 is positive, meaning increased thickness due to oxidation, then $\left(1-e^{-\frac{t_0}{t}}\right)e^{-\frac{t_0}{t}}$ varies between 0 and -0.25. To establish a maximum we must minimize t_0/t. A natural lower limit is $1/5$, which would represent a single monolayer contamination in a barrier five monolayers thick. This would leave the modified determinant approximately equal to $2\ d_0^2$. An upper bound is established by taking the variance of the mean to be a typical value for the modified determinant. The approximate maximum is 60 nm, which when doubled to effect the diameter is of order 0.1 μm. This implies that while the entire junction is shrunk by $50-100$ nm from oxidation, additional oxidation effecting barrier thickness is limited to about 60 nm of penetration.

Cryogenic testing of Josephson junctions is very important for providing feedback for fabrication. Values for normal resistance and the superconducting energy may be extracted from the current-voltage trace of the junction, both of which are unattainable at room temperature. The critical current may then be calculated from these results. When this value is compared across many junctions on the same chip, values for critical current density and process bias may be calculated. These values are shown to vary across each wafer. Adopting a model of perimeter pollution allows for the determination of an upper limit of barrier pollution, which is shown to be approximately 0.06 μm. Summary values for all variables attained from cryogenic testing are shown in table (3.4).

Variable	Range	Average
R_N	0.10 - 863 kΩ	13.88 kΩ
V_{knee}	2.85 - 4.49 mV	3.12 mV
V_{subgap}	2.43 - 3.11 mV	2.92 mV
Δ	1.33 - 1.63 meV	1.51 meV
J_c	0.10 - 181 $\left(\frac{\mu A}{\mu m^2}\right)$	4.88 $\left(\frac{\mu A}{\mu m^2}\right)$
δ_0	-0.80 - 0.67 μm	-0.35 μm

Table 3.4: Summary of values from analysis. Some outliers were discounted in the range determinations, but only those that were clearly mistakes of fitting. These statistics encompass all 391 junctions used in analysis.

Chapter 4

Apparatus for ^{3}He Refrigerator

In addition to testing and characterization of niobium junctions at 4.2 K, I participated in an effort towards building an apparatus for testing niobium and aluminum superconducting devices at 300 mK. The laboratory is already in possession of an Oxford ^{3}He refrigerator, but there were no electronics to allow for the testing of single chips. I began the design and construction of a circuit similar to that of the ^{4}He testing circuit, but with many improvements and additions. The circuit is given in figure $(4-1)$. Descriptions of each major device follows.

4.1 Battery Boxes

Low noise devices requires power supplies that are electrically isolated. One notorious source for noise is the common 60 Hz power supply. To remove the electronics from this noise, I designed and built battery boxes to provide floating power supplies. These were designed with extra care to be isolated from sources of noise.

The batteries are built into custom rack mounted aluminum boxes. A schematic of the rack mounted box is shown in figure $(C-2)$. The welded aluminum exterior creates a faraday cage to expel most electromagnetic fields that could induce noise. Conducting tape was placed on all seams to further provide a seal. Each rack mounted box has space for the electronics and batteries associated with two power supplies. A circuit diagram of the power supply system is shown in the appendix $(C-1)$.

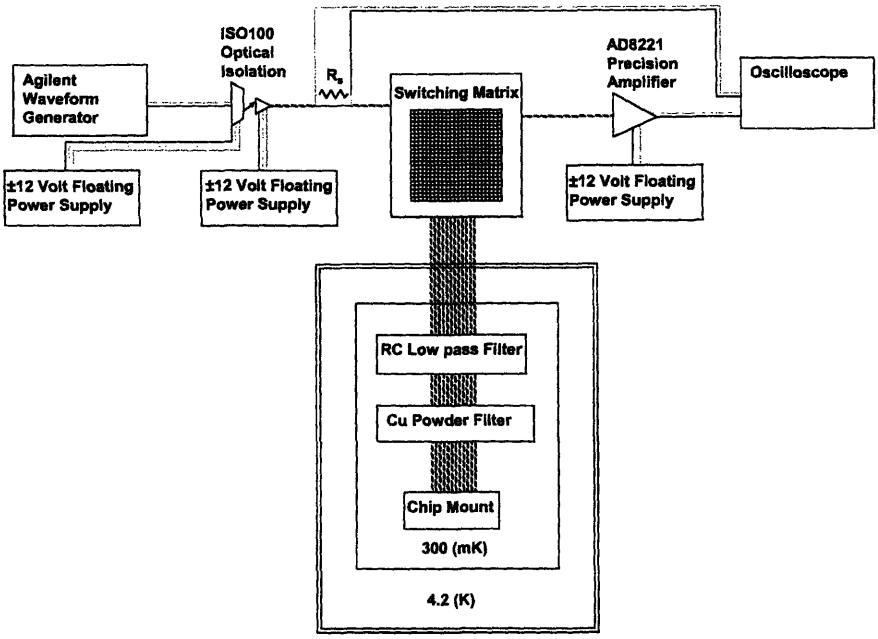

Figure 4-1: A diagram of the 300 mK refrigerator fitted to analyze devices. Each component is discussed in more depth in Chapter (4). The voltage across the source resistor gives a current reading for the oscilloscope and the amplified voltage from the chip gives the voltage reading for the oscilloscope.

The devices in use call for ± 12 Volt DC power supply. Each power supply has four rechargeable 12 V batteries. Two batteries are attached to each polarity. The box is designed to accommodate a variety of options. Any number of four independent devices can be switched on at any time. These devices are the batteries, the output, input BNC plugs, and a panel voltmeter. Feeding the appropriate voltage into the input BNC's charges the batteries. the inputs have diodes to prevent reverse flow.

The output is fed through two 5-A fuses to Amphenol 5-pin plugs. This is in conformance with the laboratory's standard for power cables. The output also has a switch that turns on LED's which indicate presence of power across output ports, which can be used to check if the fuses have been blown. The battery boxes also have the option to tie the battery ground to chassis ground or to float the ground. In addition, each battery box contains the a switch to tie the two source grounds together.

4.2 Switching Matrix

We use a 25x25 channel switching matrix to quickly change connectivity between different pins of the chip being tested. The switching matrix is mounted by two horizonal struts inside an aluminum box. The back of the box has plates that have holes for plugs. The refrigerator side of the matrix is brought in by a 25-pin D-Sub plug. This plug is connected to the matrix by twelve twisted pairs of wires. The room temperature side of the matrix is brought in by twelve twin axial plugs. These are then connected to the matrix by twelve twisted pairs of wires. A future improvement is to incorporate a Fischer plug into the matrix. Fischer plugs have better shielding than standard D-Sub plugs.

The 25th channel in both sides is tied to chassis ground. Connecting two channels is achieved by pushing a small pin into the hole at their intersection on the matrix. Pushing in multiple pins can allow for shorting channels to protect the device, or connecting channels to ground.

4.3 High Precision Instrumentation Amplifier

I designed, built, and tested an amplifier circuit to amplify the voltage signal from the chip. The signal from the chip is between a few μA and a few hundred μA and under 5 mV.

The selection of the actual amplifier was based on a minimization of offset voltage error and minimization of noise. For compatibility with existing hardware, the amplifier also had to function with input voltages of $\pm$12 V. The best model that fit these criteria was a device produced by Analog Devices Incorporated, the *AD*8221. This is a high-precision instrumentation amplifier. Its gain is adjusted by changing a gain resistor. The amplifier functions at room temperature and is mounted in a custom circuit board inside an electronics box mounted on the rack. The circuit board diagram is shown in figure $(C-7)$.

While the device has the ability to function at the floating ground provided by the batteries, an additional switch allows for this ground to be linked to chassis ground. Another switch shorts the positive and negative input channels. This can be used to protect electronics from charge built up across the input.

Both input channels are fed through single-pole RC high-pass filters before reaching the amplifier. The dropping point for this filter is 1.6 Hz. The filter is partly required because the amplifier requires a connection from each input line to common ground. The restriction on low frequency is tolerable, because the device will be operated at frequencies higher than 1.6 Hz.

For testing Josephson junctions, a gain of 1000 is used. Thus, the amplifier will boost the millivolt signal into the Volt range. When this device is operating at its maximum gain of 1000, there is a restriction in maximum frequency. The specification sheet predicts that the amplifier will start to lose its gain near 10 kHz. Testing involving this device must fall between 1.6 Hz and 10 kHz.

Source voltages of $\pm$ 12 V are used to power this device. Two decoupling capacitors connect each polarity to ground. A 0.1 μF ceramic surface mount capacitor is placed directly adjacent to the power pins of the amplifier chip. A tantalum 10 μF capacitor

is placed further away down the power line. These decouple the power lines from noise and signal generated in the device.

The board is mounted with stand-off legs in a small aluminum box. The box has three external connections, a Twin Axial BNC connection that feeds to the input, a BNC connection that runs from the output, and a five pin Amphenol connection that carries the power supply. The aluminum box allows for electromagnetic shielding, and the device is held from vibrations by the stand off legs.

Testing this device is important both to ensure that it is functioning as expected, and also to obtain a value for systematic error for its output. Gain and voltage offset are important values to characterize.

A value for gain and error in gain can be obtained by comparing input and output signals at different input voltages. A sine signal of frequency 100 Hz will fall in the middle of the amplifier's optimal frequency response. Peak-to-peak voltage input values of 2 mV, 4 mV, and 5 mV are used. Both the amplifier's input and output are saved on the oscilloscope and fit to sine curves. An example of the input output trace comparison is shown in figure $(A-11)$.

Gain is determined by use of the characteristic equation of the amplifier, $V_{out} = V_{in}A + V_{off}$. The gain of the amplifier is therefore the slope of V_{out} vs. V_{in}. The slope of this line is found to be $A = 1001 \pm 0.27$. This represents a very small systematic error in gain, of order 0.1%.

The voltage offset is also of concern. This is the voltage produced when the input is shorted to ground. This error is obtained by shorting the input and recording the output on the oscilloscope. A segment of this trace is recorded at the maximum voltage resolution of the scope. A histogram of these output voltages is shown in figure $(A-13)$. The noise fits a gaussian very well, indicating the stochastic nature of the error. The Gaussian has a mean of $-7.5\ mV$ and a variance of $2.6\ mV$. The mean translates to a value for average voltage offset and variance corresponds to the spreading of each point. With outputs of at least 1 V, an offset of this order corresponds to less that 0.1% in systematic error.

The final test of the amplifier is to obtain an estimation of the frequency response.

The Agilent current source is set to ramp the frequency logarythmically from 10^{-2} Hz to 10^{6} Hz in 9 second intervals. The signal is a 2 mV peak to peak sine wave. Both the signal and response of the amplifier are shown in figure $(A-14)$. The output signal illustrates the frequency response of the amplifier. The presence of the high-pass filter eliminates the signal below 1 Hz. The amplification begins to attenuate above 10 kHz as predicted by the specification sheet. This frequency response is sufficient to capture the frequencies of relevance to Josephson junction testing.

When this device is operated within the valid frequency range, it can be counted on to provide a signal with very good accuracy. Other sources of error will be more significant than the order 0.1% gain error. The offset error can be marginalized by sweeping current up and down the voltage axis in the same way offset errors are nullified in the ^{4}He apparatus.

4.4 Optical Isolation

I designed, built, and tested an optical isolation circuit for a current source for use in device testing. An optical isolation amplifier converts an electrical signal into photons generated by an LED and, subsequently, received by a photo detector. The photo detector reconstructs the signal with some predetermined gain. This process is most useful in creating a signal with a new isolated common ground. Unity gain will be used in this case so the device will simply serve to separate the signal from the ground of the Agilent signal generator. The Agilent uses 60 Hz wall power so it is subject to both 60 Hz noise and coupling to all other electrical equipment on the circuit.

The device used is the Burr-Brown ISO100CP optical isolation amplifier. This device was selected because of the group's familiarity and satisfaction with its operation. Similar digital isolation devices have less desirable noise and bandwidth. This device operates in unipolar or bipolar modes depending on how the circuit is wired. Bipolar mode will be used to view the symmetry of the devices and negate offset errors. A circuit board diagram is shown in figure $(C-8)$.

Achieving bipolar mode is achieved by adding a bias current to the input to shift

the 0 input mark at the middle rather than the lower end of the device's current range. The bias current is created by an internal current source and adjusted with a potentiometer. This allows for fine tuning of the output bias.

Another potentiometer is used in the input side connecting a reference channel to ground. This adjusts an internal bias current in line with a feedback photo receptor also receiving the signal from the LED. Adjusting this potentiometer changes the value of input current bias and shifts the 0 input mark.

The isolation amplifier is a current matching device which is designed to match the current in with the current out, in the case of unity gain. This functionality is converted into a voltage matching device by adding gain resistors to the input and output lines. The ratio of these resistors designates gain, so picking them to be equal specifies unity gain. A potentiometer in series with the large, 316 kΩ, gain resistors serves to fine tune the gain.

The Optical Isolation device requires two independent power supplies to function properly. Both the input and output sides require the $\pm$12 Volt power supplies provided by the batteries. Like the amplifier, two decoupling capacitors are used in each polarity of each power supply. A 0.1 μF ceramic surface mount capacitor is connected from ground to the power pins on the chip. A larger 10 μF tantalum legged capacitor is used further away from the chip.

The frequency response of the isolation includes a second order peak at 34 kHz. To reduce the effect of this, a capacitor is put in parallel with R_F, the output gain resistor. The effect of this should be a pole cancelation that removes this peak.

The design for this circuit was largely taken from design suggestions in the manufacturers literature. Selection of this design was based on minimization of error. The three potentiometers in this design can be used to minimize the output offset and gain error from this device. This is accomplished by first turning off the input and trimming the input current offset, then adding an input and trimming the gain potentiometer and voltage offset potentiometer to minimize gain and offset error.

This device is tested in the same way as the precision amplifier is. It is important to obtain a value for gain, gain error, and offset as well as the approximate frequency

response. The first test is of the frequency response. Like the amplifier, the frequency is ramped logarythmically from 10^{-2} Hz to 10^{6} Hz with a 9 second period. The signal is a sine wave with peak to peak voltage of 2 Volts. The signal and response are shown in figure $(A-15)$. The test shows unity gain from DC to around 34 kHz where there is a peak before the device gain attenuates. The peak is predicted by the specification sheet. A capacitor in parallel with the output gain resistor should have reduced it. The peak should not have much of an effect, however, because other devices in the circuit filter frequencies higher than that out.

To be assured of the validity of the circuit, it is necessary to test the gain and offset error of the amplifier. Both of these are done in the same way as in the precision amplifier. The voltage offset is tested by measuring the output when the input is shorted. A histogram of this signal's voltage values is shown in figure $(A-13)$. While the data does not fit a gaussian, a mean can be calculated to be 4 mV with an estimated variance of 6 mV. With voltage signals of at least a volt, this represents systematic error less than 0.4% which decreases for higher signal voltages.

To test the gain, the input and output of different amplitude sine waves are compared. The device will be operated in the volt regime to minimize the effects of offset error, so sine waves of input amplitudes 1 V, 2 V, 3 V, and 4 V are recorded. The inputs and the outputs are fitted to sine waves and the amplitudes are compared. In a similar way as the amplifier, a line may be fitted to V_{in} vs. V_{out}. The slope of this line is the gain. This value is found to be 0.996 ± 0.007. The amplifier can not output a signal higher than 4 V in the positive domain, but can go higher than 10 V in the negative domain. These limitations must be kept in consideration when testing. Errors in gain translate to another 0.4% systematic error that does not change with higher signal value, until 4 V at which point the device is above its operating range. The isolation can function between DC and 30 kHz with input voltages under 4 Volts with unity gain of error less than 1%.

4.5 300 mK Electronics

I designed and built a single pole RC filter to operate at 300 mK. The device has 24 channels, each with an independent filter. A 10 kΩ thin film resistor and 1 μF ceramic thin film capacitor create a cutoff frequency of 16 kHz. The circuit elements had to be selected for maintained functionality at 300 mK.

The device is contained in a box constructed of Oxygen free hard copper covered in gold. The box is 1.3" by 1.3" by 0.8". It is designed to be very small, so that it can fit on the thermal finger. The ends are almost completely covered with the d-sub mini plugs. To conserve space the board is divided in half and mounted back to back with a layer of gold coated copper in between. This allows for convenience in wiring as well as more efficient space usage and thermal dissipation. The filters are designed to block noise coming from room temperature. A schematic for the copper box to hold the filter is shown in figure $(C-4)$ and the circuit board diagram is shown in figure $(C-6)$.

The thermal finger that holds the chip has mounting slots for two copper powder filters. The mount and the filters were designed by David Berns. A design schematics for the the thermal finger is shown in figure $(C-3)$ and a schematic for the copper powder filter is shown in figure $(C-5)$. Each filter has six holes. A twisted pair of wires is fed through the hole then the hole is filled with a fine copper powder. This serves as a low pass filter with a cutoff frequency around 1 GHz. This filter is necessitated because RC filters switch functionality at extremely high frequencies, thus at higher than a few GHz, the RC low pass filter may behave as a high pass filter.

The chip itself is mounted on a gold coated copper rod. The end of the rod has threading that is used to attach a small chip holder. The chip mount was designed by David Berns. I designed and built an adapter that allows the chip mount to attach to the thermal tongue on the Lincoln Laboratory refrigerator.

4.6 Other Room Temperature Electronics

I designed and built a variable resistor which is used to control the current that it sent to the device. This resistor is designated R_s and is a rack mounted device. The device features six resistors in decades between 100 Ω and 10 MΩ. Both BNC and twin axial connections on both sides of the resistor allow for splitting the input and output of this device to go to both the oscilloscope and switching matrix.

Because the voltage across this resistor translates directly into the current reading by Ohm's law, discrepancy in resistance translates to systematic error in current reading. For the 100 Ω through 1 MΩ resistors, use of high precision devices minimizes the error. The resistors have measured resistances within 0.5% of the expected amount. the 10 MΩ resistor is not a precision resistor and the error is 3.5%. This systematic error must be taken into account when measuring current.

A cable is needed to connect the refrigerator to the switching matrix. I constructed a custom cable for this task. The connection on the refrigerator is a 24 pin Fischer plug. There was no preexisting connection on the switching matrix. A 25 pin D-sub connection proved to be a convenient choice. A future improvement of this apparatus would be to add a Fischer plug to the switching matrix because the Fischer plugs have better shielding.

The cable itself is 6.5 feet long. It is comprised of twelve twisted pairs of wires surrounding by a metal mesh sheath. The sheathing mates with the Fischer connection and d-sub on the other end. For further electromagnetic shielding the d-sub plug, which is made of plastic, it is covered in conducting tape. A layer of shrink wrap is used inside the Fischer connection to prevent the solder junctions from touching the metal shielding.

This apparatus incorporates both twin axial and BNC cables. Flexibility in switching between these cable types is important to guarantee this custom equipment be versatile. To facilitate switching between BNC and twin axial cables, I constructed a box to switch between BNC and Twin axial. The box has three separate channels and uses twisted pairs of wires to connect them.

4.7 Testing Room Temperature Apparatus

A good test of the room temperature electronics is to use them to verify established 4.2 K data. The Peterson probe, as described in section (2.2), can be used with the equipment I built and designed. A schematic of this modified apparatus is shown in figure $(A-16)$. This apparatus incorporates the isolation amplifier, resistor box, amplifier, and miscellaneous electronics used at room temperature. While this is an indication of systemmatic problems the values should not be used as a strict error estimation. The apparatus is designed for use with a setup with twinaxial connections, not the BNC present on the Peterson probe. In addition to this, the current estimation assumes the junction and line resistances to be negligible, which is not a valid assumption. A final difference is the oscilloscope, an averaging analog scope is used for the regular setup, while the testing apparatus uses a digital oscilloscope for ease of data collection.

With these things in mind, this test is to provide a proof of functionality. Current-voltage traces of a junction tested in both setups is shown in figure $(A-17)$. The junction is observed with the new apparatus. Agreement with the voltage dependant Δ measurement is better than agreement with the current and voltage dependant measurement for R_N. This is expected because the current measurement ignores line resistance and that of the device, whereas the voltage measurement should still be accurate.

Chapter 5

Future Plans and Concluding Remarks

5.1 Summary

The goal of this thesis is to investigate the properties of Josephson junctions to provide feedback to facilitate process development of fabrication. This endeavor begins with macroscopic theory and microscopic results that provide the foundation of superconductivity. The Josephson equations are derived in terms of an unknown coupling. The results of Ambegaokar and Baratoff provide a value for this coupling [19]. Two barrier geometries are then compared to aid in characterization of junctions. The final theoretical preparation is a numerical simulation of the self-limiting magnetic field of junctions of circular cross section. Results of this simulation agree with literature and conclude that this effect does not impact junctions of the size tested in this thesis.

All cryogenic data I collected for this thesis was done with an existing 4 K cryogenic probe. This apparatus and chips tested are described in chapter (2). The description of the chips and likely junction fabrication features includes discussion of feedback that would be helpful to fabrication. This includes process bias δ_0 and critical current density J_c. These factors, along with the others discussed, cannot be determined accurately at room temperature. The apparatus is then presented along with the custom software used to analyze the data collected. Example junction

current-voltage traces are shown and the methods of analysis are described. The software and methods used to analyze the aggregate data is also described.

The next section describes the analysis and results of both the wafer and junction aggregates. First R_n and Δ are extracted from the current voltage trace. The value for Δ is in good agreement with other experiments given the considerations of material inhomogeneity. Methods for determining the process bias and critical current density are presented. Using the simple model, typical values for these parameters are calculated. These values vary heavily across wafers, but they have a clear mean which is presented with all the results from this section in table (3.4). A second model of junction barrier is then used to establish a bound on perimeter pollution depth of the barrier. This value is found shows a believable upper bound for this value. It is clear that neither of these models accurately describe the barrier and that the data set is too limited to provide a clear picture. These models are useful in their feedback to process testing so that fabrication parameters may be adjusted to improve the quality of junctions produced.

The final section of the thesis describes the apparatus built that will allow for testing at 300 mK. Major steps have been taken to construct and test an amplifier, isolation amplifier and supplementary circuitry at the room temperature level. In addition an RC filter has been built that functions at 300 mK as well as much of the physical apparatus to hold the chip. This apparatus has been used to verify 4.2 K testing done by the old apparatus. This testing has provided a useful check of the room temperature electronics and demonstrated the apparatus's readiness to move to 300 mK.

5.2 Future Plans

Constructing an apparatus for testing devices at 300 mK is interesting in many ways. For the purposes of testing the niobium trilayer junctions, having a lower thermal threshold gives many advantages. Thermal spreading of features will be decreased by a factor of 10, which increases the precision of features like Δ. This refrigerator

will enable testing at temperatures below the critical temperature of aluminum, 1.175 (K) [2]. Being below T_c for aluminum could change the way the aluminum in the niobium barrier behaves. If indeed it is behaving as a superconductor due to the proximity effect, than there will be no change. If it is functioning as part of the barrier, the aluminum will become superconducting and will contribute to the junction. Barriers between superconductors with different superconducting gaps have different characteristics [2].

The lower temperature will more than just allow for lower noise. Techniques have been demonstrated for measuring barrier homogeneity at temperatures near 1.2 K [28]. Barrier homogeneity is one of the crucial pieces of feedback the fabrication development process needs. Testing at this temperature would be invaluable to fabrication. There is also predicted subgap structure that should be visible at this temperature. A conductance spike at $2\Delta/3$ has been shown [28]. Also of interest is the possibility of observing the quantization of conductance in the sub-gap region by observing subsequent resistive channels open up. This has been observed in atom-size contacts [29].

In addition to helping with fabricating niobium trilayer junctions, The Analog Device Technology Group at Lincoln Laboratory is also involved in an initiative to produce aluminum trilayer junctions. These will not be testable above the critical temperature of aluminum. Functioning aluminum trilayer junctions built for quantum computing applications have only been realized by the DSM project at Lincoln Laboratory. Room temperature characterization looks promising.

Besides improvements solely due to lower operation temperature, the 300 mK apparatus will have better isolation, better filtering, and, therefore, better noise than the setup currently used to test cryogenic circuit elements. While the current setup is not designed to function optimally with the Peterson probe, if the need arises for more precise electronics to test junctions at ^{4}He temperatures, this apparatus can be adapted.

A final improvement 300 mK He^3 brings to the groups experimental capabilities is the use of a heater. The refrigerator is fitted with a heater that can control the

temperature between 300 mK to 4.2 K. This sort of thermal control allows for the testing of the thermal dependance of parameters. Of particular concern is exploring the temperature dependance of the superconducting gap especially when crossing the T_c of aluminum.

Appendix A

Figures

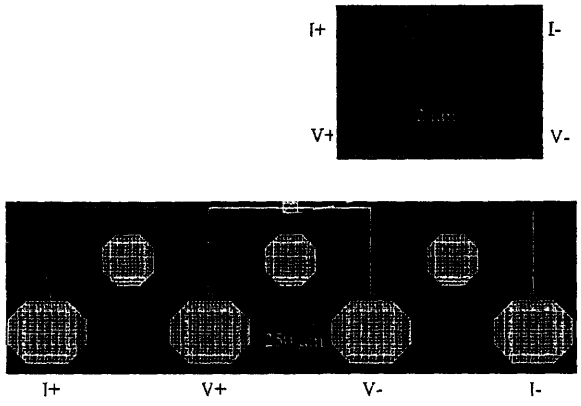

Figure A-1: A diagram of a test structure that shows the connecting pads for a single Josephson junction. The inset shows the relative scale of the actual junction to the pads.

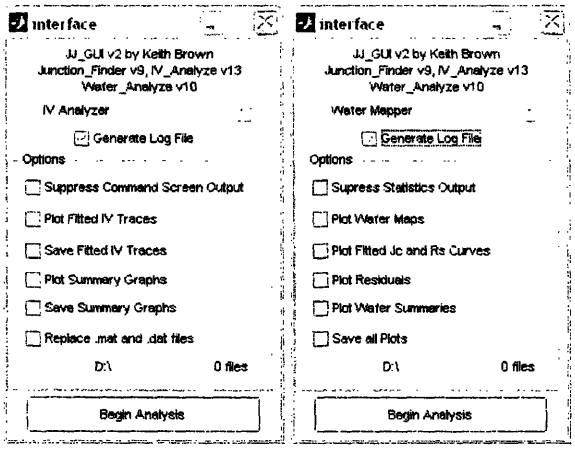

Figure A-2: Graphical user interface (GUI) of the custom MatLab software developed for the LTSE and DSM project. The drop box has two options of what to analyze, the two images show these two options. The check boxes control what the program analyzes and saves.

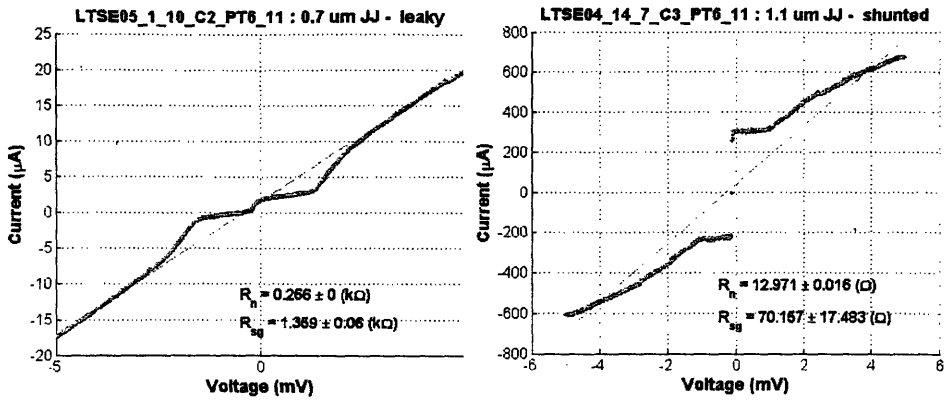

Figure A-3: Two failure modes of Josephson junctions that are caught by analysis. These are direct output plots of the program. The left junction is leaky, where resistive channels are present across the insulating barrier. The second is shunted. These failure modes are distinct but do not reveal exactly which fabrication problem they represent. The red points on the graph indicate points used for fitting.

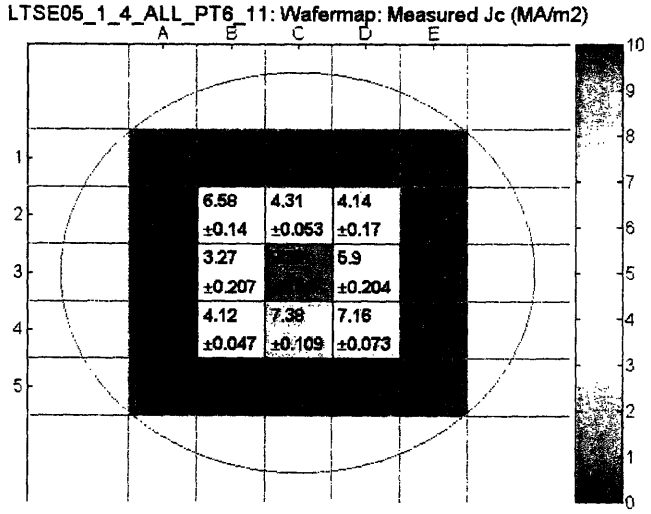

Figure A-4: An example wafer map measuring critical current density. The blank squares indicate that either no chips were tested from that die or that there were not enough valid junctions to determine J_c.

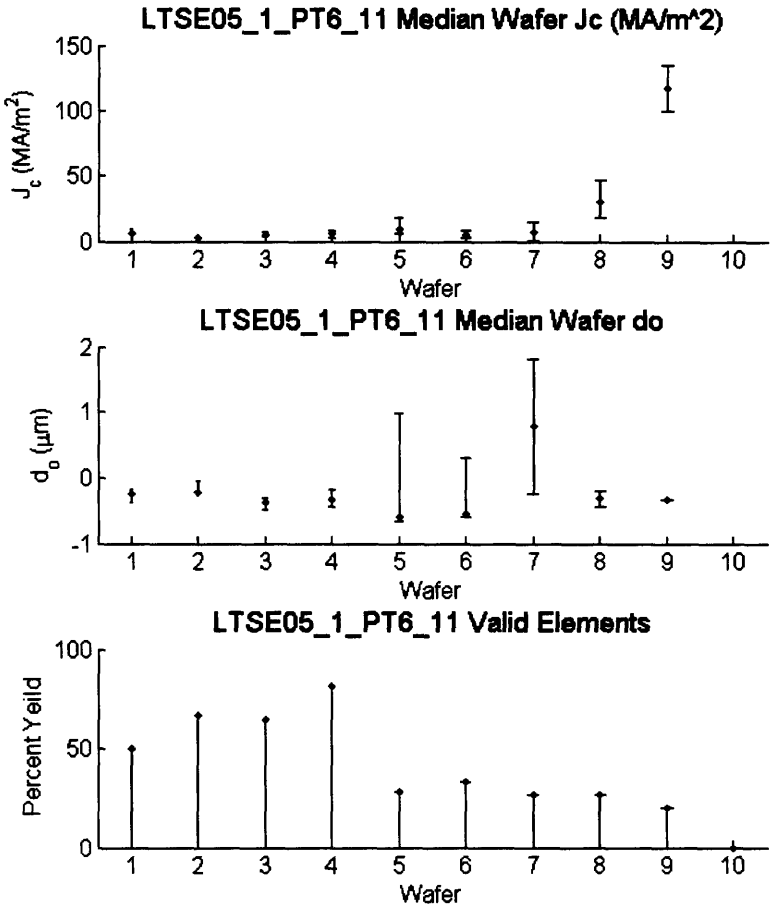

Figure A-5: Plots of fitting averages across a single run. In these plots, LTSE05_1 is summarized. In the plots of average δ_0 and J_c the error bars signify the range of the value from each wafer. The expected J_c was 5 $\frac{\mu A}{\mu m^2}$ for wafers 1 through 8.

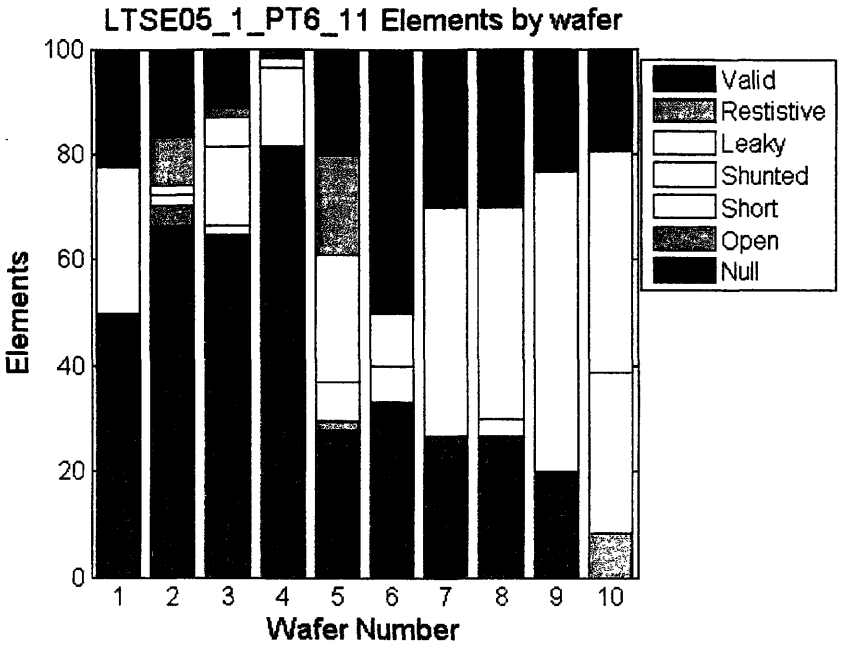

Figure A-6: A bar graph that shows distribution of junction type and failure mode by wafer number. This makes it clear what kind of failure modes were dominant on each wafer.

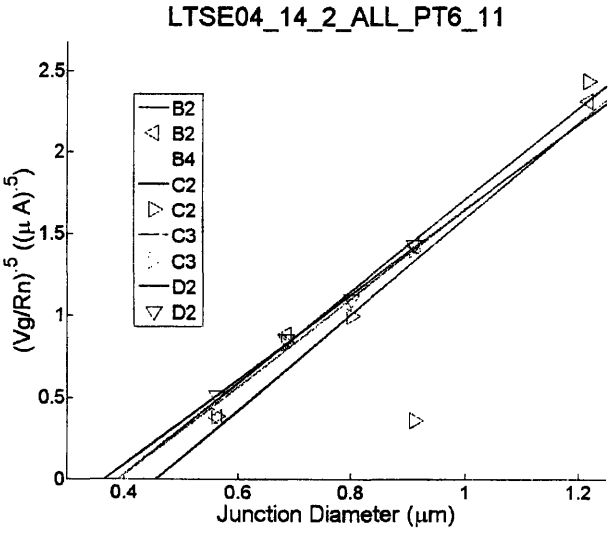

Figure A-7: A plot of the fitted $\sqrt{I_c}$ vs. δ. An entire wafer of data is shown here, with individual die differentiated by different colors and direction triangles. Triangles with a red 'x' inside them signify that the point was not used for fitting, either due to a of lack of points or it was determined to be an outlier.

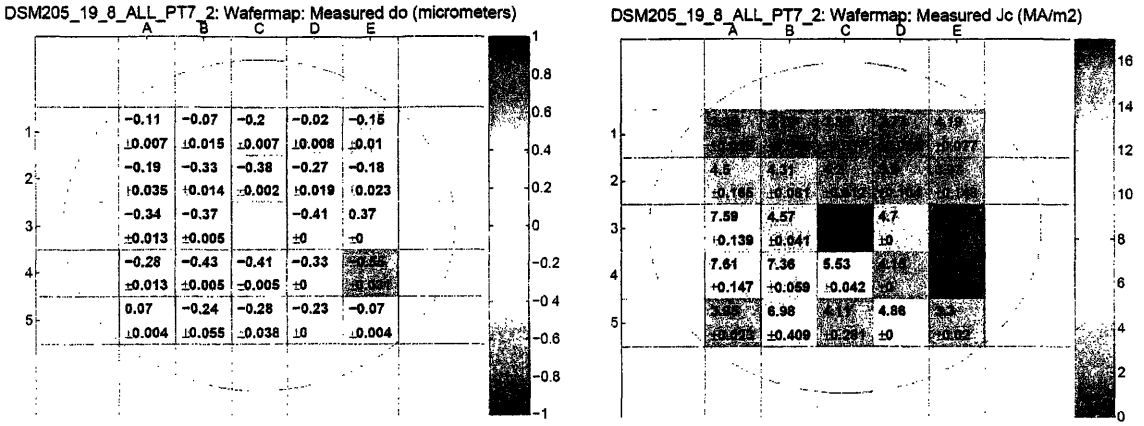

Figure A-8: Data from the DSM2_19_8 wafer. Every chip on the wafer was tested and the yield was high, making it an ideal wafer to look at trends across the wafer. Error reported is error in linear fitting. Traits that are reported with zero error indicate only two functioning junctions, allowing for a perfect linear fit, while there is no error in fitting.

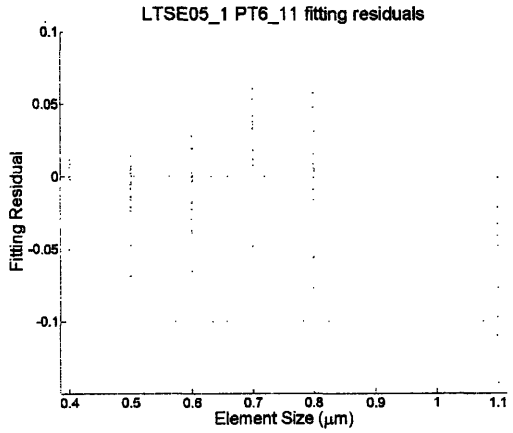

Figure A-9: Fitting residuals plotted against junction diameter. There are noticeable trends in the average residual for a given diameter. The residual would be centered about 0 if the noise was random.

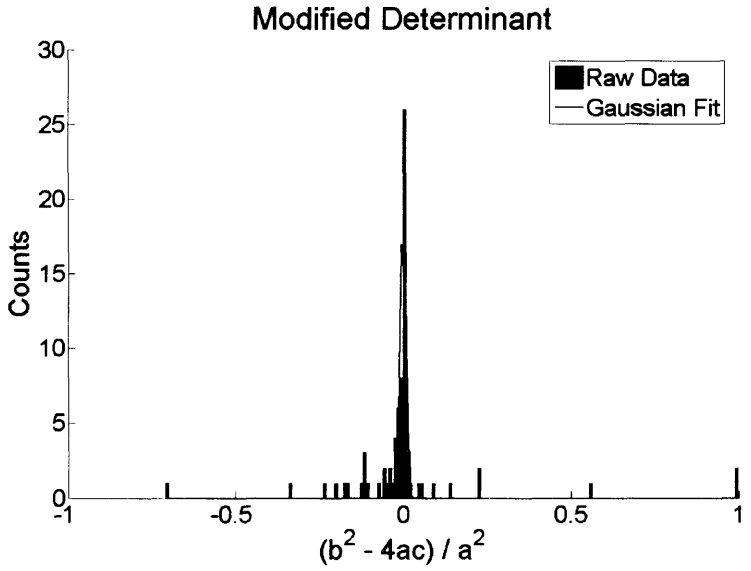

Figure A-10: Histogram of the modified determinant with a gaussian fitted to it. The mean is $-.0010 \pm .0079\ \mu\text{m}^2$.

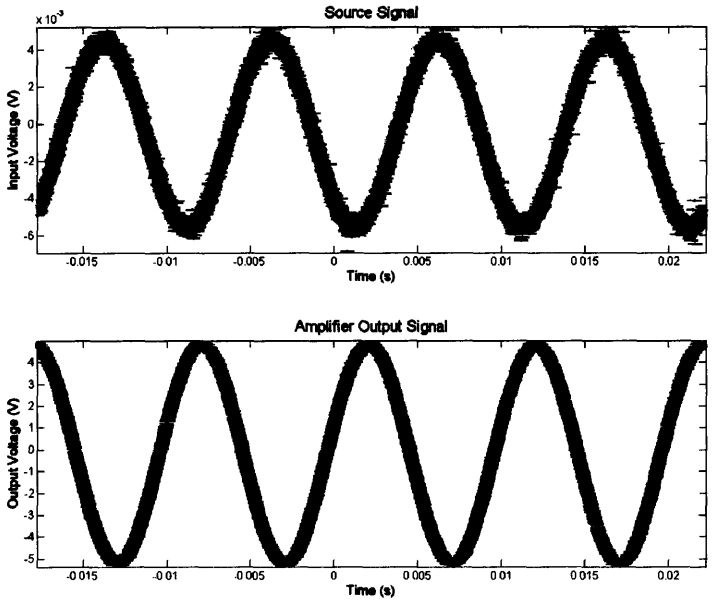

Figure A-11: Example of voltage vs. time plots from the output of the waveform generator and from the amplifier. While the input amplitude is the same for both plots, the phase is different because the measurements were taken at different times. The amplifier presents a 10 kΩ load resistance, which greatly dominates the source resistance of 50 Ω. Internal scope resistance of 1 MΩ is used to get a similar load for the scope.

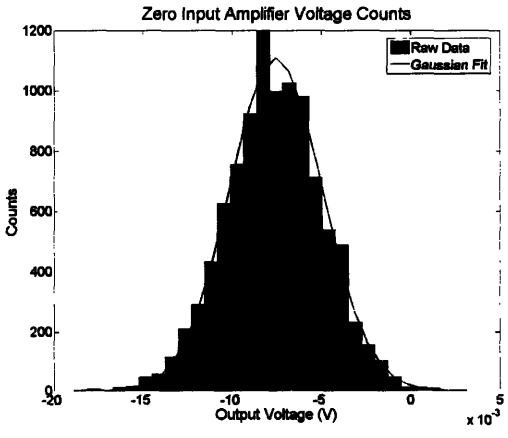

Figure A-12: Histogram and Gaussian fit of zero input voltage readings of the AD8221 amplifier.

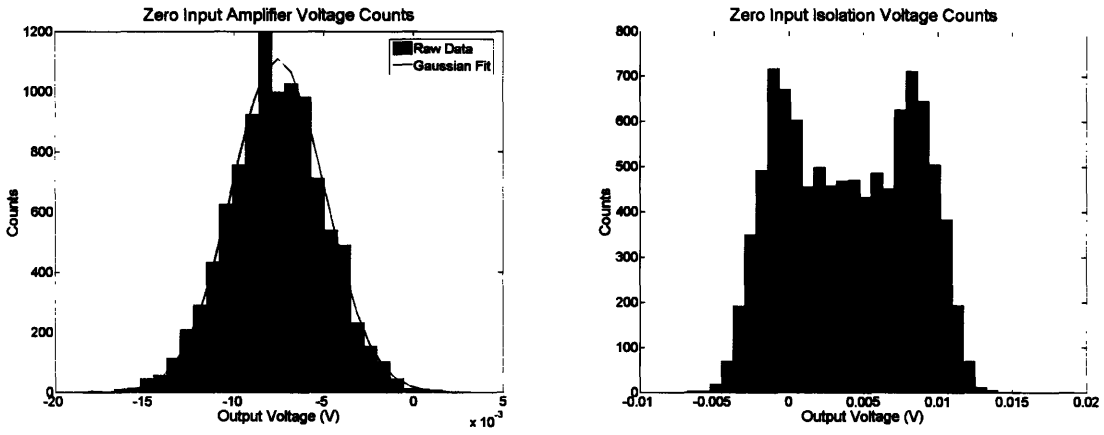

Figure A-13: (Left) Histogram and Gaussian fit of zero input voltage readings of the AD8221 amplifier. (Right) Histogram of zero input voltage reading of the optical isolation amplifier. The voltages do not fit a gaussian, but the mean is 4 mV and the variance can be approximated by 6 mV.

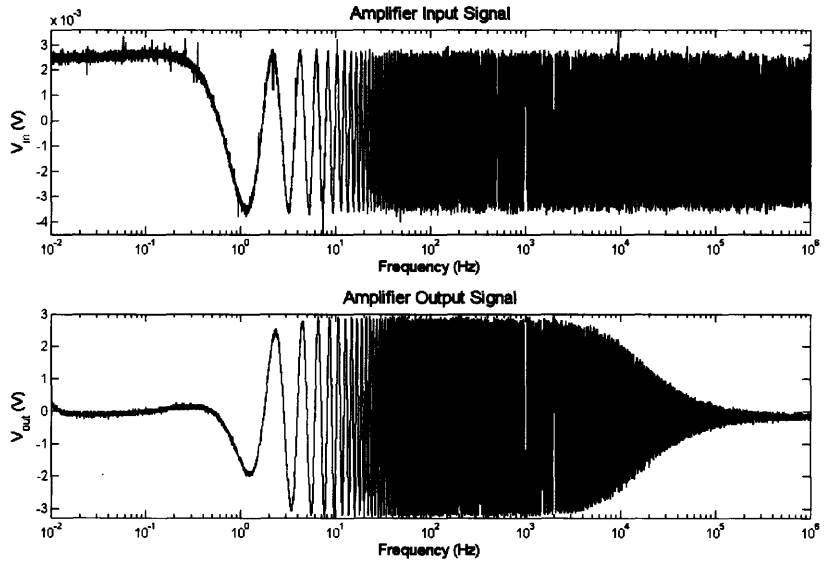

Figure A-14: The top graph is the frequency ramped sine wave input to the amplifier. The bottom graph is the output of the amplifier. The The envelope of the bottom graph is the frequency response of the device.

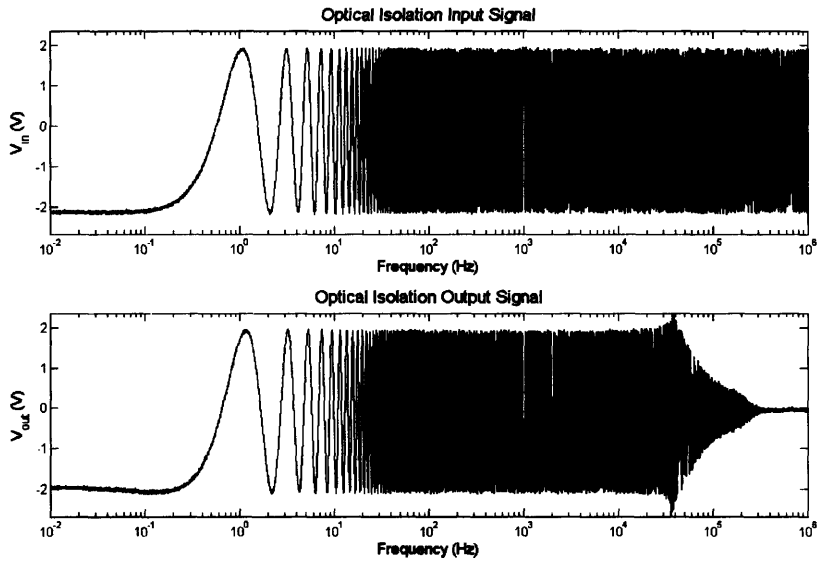

Figure A-15: The top graph is the frequency ramped sine wave input to the optical isolation amplifier. The bottom graph is the output of the optical isolation amplifier. The The envelope of the bottom graph is the frequency response of the device.

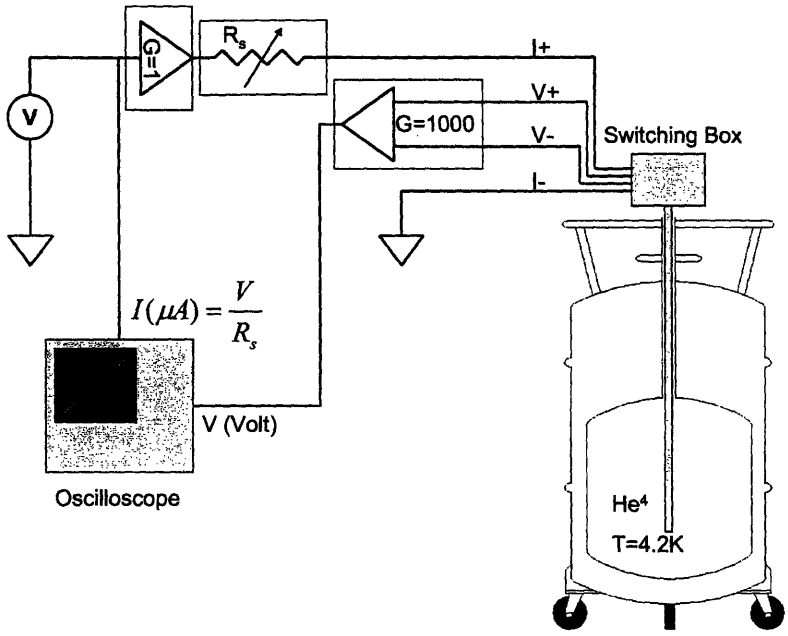

Figure A-16: 4.2 K Peterson testing apparatus modified with custom electronics for the purpose of verifying the electronics. Components in shaded boxes indicate that they were designed and tested for this project.

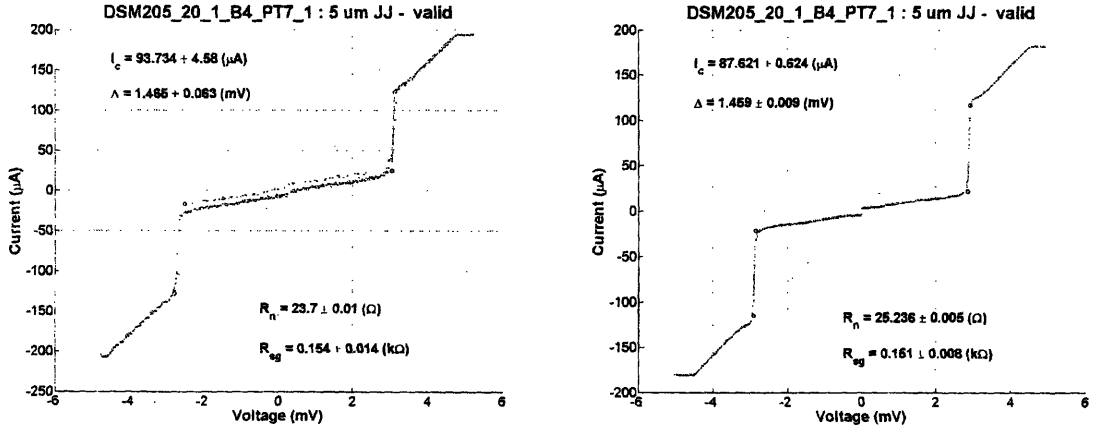

Figure A-17: (Left) Current-voltage trace of a Josephson junction taken by the custom apparatus described in figure $(A-16)$. (Right) Current-voltage trace of the same Josephson junction taken by the apparatus described in figure $(2-2)$.

Appendix B

MatLab Code

B.1 Self-Limiting Induction Effects

```
%Simulation to determine Self Limiting Field Effects
%of Josephson Junctions of circular geometry
%
%Written by Keith Brown 5.10.2006

clear; junction_radius = logspace(-3,log10(5),1000);
                                          %Junction sizes to try
initial_phase_guess = logspace(-1,log10(pi./2),1000);
                                          %Range of phase values to try
step = .0005;                             %Iteration step size in l

for i=1:length(junction_radius)           %first iterate size
    for j=1:length(initial_phase_guess)   %Then iterate initial phase
        steps = round(junction_radius(i)./step-1);
                                          %keep step size constant
                                          %across sizes
        l=linspace(step,junction_radius(i),steps);
```

```
                                        %sweep the radial variable, l
        p=zeros(1,steps);               %Phase Variable
        p(1)=initial_phase_guess(j);    %seed initial value
        dp1=zeros(1,steps);             %first derivative of phase wrt l
        dp2=zeros(1,steps);             %second derivative of phase wrt l
        Ienc=zeros(1,steps+1);          %inclosed current
        for k=1:steps-1                 %vary l from inside out
            Ienc(k+1)= Ienc(k)+2.*pi.*sin(p(k)).*l(k).*step;
                                        %determine enclosed current
            dp1(k)=Ienc(k+1)./(2*pi*l(k));  %first derivative from amperes law
            dp2(k)=sin(p(k))-dp1(k)./l(k);  %second derivative from
                                        %differential equation
            p(k+1)= p(k) + dp1(k).*(step)+.5.*dp2(k).*step.^2;
                                        %iterate phi with Taylor expansion
        end
        I_phase(j) = Ienc(length(Ienc)-1);  %carry max current for each
                                        %initial phase
    end
    [Imax(i) j_index] = max(I_phase);   %remember max current and best phase
    best_initial_phase(i) = initial_phase_guess(j_index);
end

figure;                                 %plot best initial phase vs. size
hold on plot(junction_radius,best_initial_phase,'.')
title(['\phi_{s=0} that gives maximum I_c'],'fontsize',16);
xlabel('r/\lambda_J','fontsize',16);
ylabel('\phi_{(s=0)}','fontsize',16);
legend(['\phi_{s=0}of maxI_c']);
axis([0,max(junction_radius),0,pi./2])
```

```
figure;                                          %plot max current vs. size
hold on plot(junction_radius,Imax,'b.')
plot(junction_radius,pi.*junction_radius.^2,'r-')
                                                 %plot against unbiased curve
title(['Size of Junction vs. Maximum I_c'],'fontsize',16);
xlabel('r/\lambda_J','fontsize',16);
ylabel('Ic/(\lambda_J^2J_c)','fontsize',16);
legend('I_{max}withself inductance',...
    'I_{max}withoutself-inductance');
axis([0,max(junction_radius),0,max(Imax)])
```

B.2 Characterizing Josephson Junctions

```
function [I_knee, I_knee_error, V_sg, V_sg_error, Rn, Rn_error, Rsg,
...
    Rsg_error, I_gap, I_gap_error, V_knee, V_knee_error, type, ...
    IV_analyze_output] = ...
    IV_analyze(IV_untrimmed,word,plot_things,supress_output,element,string)
%v2 6/20 - KB - changed definition of resistive to Rsg/Rn > .7 and
%                  1.5 mean > std.
%               changed definition of null to 620 or less points from 601
%               added new check for bad lines, slope of 5,6
%v3 6/21 - KB - added inversion of R
%v4 6/28 - KB - changed line searching to center around 3, 1 volts
%               added error condition of lines 3,4 having very different
%                  intercepts
%               Changed normal resistance to look at both sides
%v5 6/29 - KB - Added error to Rn with disagreement with bounds
```

```
%v6 6/30 - KB - Changed Window for drop line to 200 points
%               Added Leaky and Shunted Distinctions to failure modes
%               Changed Window for Rn lines to 100 points each
%               Changed voltage for Rsg from 1.00 to .75
%               Basically All corrections to bring it back to 10 mV width
%               Added check to make sure Knee ranges are in IV trace
%v7 7/06 - KB - Added Strings analysis and Guided Analysis for resistors
%v8 7/12 - KB - Added cleanup function to get rid of noisy junctions
%v9 7/14 - KB - Added units to Rn and Rsg display of IV trace
%               All R valus still saved as kOhm however
%v10 7/18- KB - Added support for open and shorted junctions
%v11 7/19- KB - Modified short/open recognition to rely on middle current
%v12 7/28- KB - Modified the linear analyze to require additional input
%               Modified linaer analyze to perform better at 3mV
%               Changed input trace to IV_untrimmed from IV
%v13 8/08- KB - Enlarged font size on plots
%               added output string of characterization for logging
%v14 5/10- KB - Changed output of ongraph stats to delta and Ic
%               Changed Ic determination to be consistent with A-B relation
%               Allowed for non 1024 length IV vectors.
%For details or troubleshooting check comments within the code. This
%program is called by Junction_finder. It can currently deal with
%resistors, or any known failure mode of josephson junction. The Vgap is
%hardwired in the program to be 3mV along with other paramenters of
%fitting. If these need to be changed I recommend making global variables
%and logging any changes to the code. Different scale plots will process
%properly granted enough points are in the region of interst.
%
%Keith Brown 8/8/2005 brownka@gmail.com
```

```
warning off;

IV = trim(IV_untrimmed);
%removes single valued trailing edge left by oscilliscope
%IMPORTANT: if there is ever an error where it calls a good curve null open
%or short the error might be here, refer to the notes in trim to see why.
%It would only occur if the curve returned to the values that the scope
%trailed off at, this almost never occurs before the curve in general
%increases with voltage. See notes in trim for the solution

%add a voltage offset to center the curve about 0
if size(IV,1)>0
    volt_offset = (IV(1,1)+IV(length(IV),1))./2;
    IV(:,1)=IV(:,1)-volt_offset;
    IV_untrimmed(:,1)=IV_untrimmed(:,1)-volt_offset;
end

%initialize Variables
IV_analyze_output = '';graphFontSize=14; I_knee =0;I_knee_error
=0;V_sg=0;V_sg_error =0;Rn =0;Rn_error =0;Rsg =0; Rsg_error =0;I_gap
=0;I_gap_error =0;V_knee =0;V_knee_error =0;

%prepare the plot if plotting.
if(plot_things)
    figure;
    hold on
    plot(IV_untrimmed(:,1),IV_untrimmed(:,2),'b.')
    xlabel('Voltage (mV)','FontWeight','bold','FontSize',graphFontSize);
    ylabel('Current (\muA)','FontWeight','bold','FontSize',graphFontSize);
    set(gca,'XGrid','on','FontSize',graphFontSize-2)
```

```
    set(gca,'YGrid','on','FontSize',graphFontSize-2)
end if (~supress_output)
    fprintf(['Analyzing: ' word]);
end IV_analyze_output = [IV_analyze_output,word];

%Define scope error as (distance between closest two points)/2^.5
%In need of better systemmatic error for points collected
global inst_error; inst_error = max(IV(:,2)); for i=1:length(IV)-1
    if and(0<abs(IV(i,2)-IV(i+1,2)),inst_error>abs(IV(i,2)-IV(i+1,2)))
        inst_error = abs(IV(i,2)-IV(i+1,2));
    end;
end; inst_error = inst_error ./sqrt(2);

%calculate slope by finite difference method, single differential
for i=2:length(IV) - 1
    slope(i)=(IV(i+1,2)-IV(i-1,2))./(IV(i+1,1)-IV(i-1,1));
end;

%program records all zeros if no data is taken, trimming reduces the IV to
%null if there is no data
if all(zeros(length(IV_untrimmed(:,2)),1)==IV_untrimmed(:,2))
    shifted = false;
    if (~supress_output)
        fprintf(' - null data set\n');
    end
    IV_analyze_output = [IV_analyze_output,' - null data set\n'];
    type = 'n';
    status = ' null';
elseif length(IV)<620
    shifted = false;
```

```
[junk mid] = min(abs(IV_untrimmed(:,1)));
if mid<51
    mid = 51;
elseif mid > length(IV_untrimmed)-51
    mid = length(IV_untrimmed)-51;
end
%in null cases distinguish between open and short
if or(and(0.1>abs(mean(IV_untrimmed(1:500,2))-...
        mean(IV_untrimmed(525:1024,2)))/abs(mean...
        (IV_untrimmed(1:500,2))+mean(IV_untrimmed(525:1024,2))),...
        0.1>abs(std(IV_untrimmed(mid-50:mid+50,2))/...
        mean(IV_untrimmed(mid-50:mid+50,2)))),size(IV,1)==0)
    if (~supress_output)
        fprintf(' - Open\n');
    end
    IV_analyze_output = [IV_analyze_output,' - Open\n'];
    type = 'o';
    status = ' open';
elseif length(IV)<100
    if (~supress_output)
        fprintf(' - Short\n');
    end
    IV_analyze_output = [IV_analyze_output,' - Short\n'];
    type = 'h';
    status = ' short';
else
    if (~supress_output)
        fprintf(' - null data set\n');
    end
    IV_analyze_output = [IV_analyze_output,' - null data set\n'];
```

```
        type = 'n';
        status = ' null';
    end
    %this should have been already check for
elseif and((std(slope)==0),(mean(slope)==0))
    if (~supress_output)
        fprintf(' - null data set\n');
    end
    IV_analyze_output = [IV_analyze_output,' - null data set\n'];
    type = 'n';
    status = ' null';
else
    %knee closest to 3mV times number of elements in string
    [junk Vknee_index_low] = min(abs(IV(:,1)+3*string));
    if Vknee_index_low < 103
        Vknee_index_low = 103;
    end
    [junk Vknee_index_high] = min(abs(IV(:,1)-3*string));
    if Vknee_index_high > length(slope)-102
        Vknee_index_high = length(slope)-102;
    end
    %sub gap curve closest to .75mV times number of element in string
    [junk Vsg_index_low] = min(abs(IV(:,1)+.75*string));
    [junk Vsg_index_high] = min(abs(IV(:,1)-.75*string));
    midpoint = [50,length(IV)-50,Vsg_index_low,Vsg_index_high];
    %define area to look for subgap
    min_end = [1,length(IV)-100,Vsg_index_low-50,Vsg_index_high-50];
    max_end = [100,length(IV),Vsg_index_low+50,Vsg_index_high+50];
    %to tell it not to maximize the slope for these
    exp_slope = [-1 -1 -1 -1];
```

```
%cleanup solves the double value problem
%NOTE: the graph has already been displayed, the shifted values will
%not appear on the final graph but will be used in the calculations
[IV shifted1] = cleanup(IV,min_end(3),max_end(3));
[IV shifted2] = cleanup(IV,min_end(4),max_end(4));
shifted = or(shifted1,shifted2);
if and(shifted,~supress_output)
    fprintf(' - noisy');
end
IV_analyze_output = [IV_analyze_output,' - noisy'];
%%%%%%%%%%%%%%%%%%%%%%%%%%%%%%%%%%%%%%%%%%%%%%%%%%%%%%%%%%%%%%%%%%%%%%%

%calculate linear fit to the normal and sub gap regimes
for j=1:length(midpoint)
     [lines(j,1) lines(j,2) lines(j,3) lines(j,4) lines(j,5) ...
         lines(j,6)  lines(j,7)] = findlinear(IV,midpoint(j),...
         round((max_end(j)-min_end(j))./4),min_end(j),...
         max_end(j),exp_slope(j));
     if (plot_things)
        plot(IV(lines(j,4):lines(j,5),1),lines(j,2).*...
            IV(lines(j,4):lines(j,5),1)+lines(j,3),'-r','LineWidth',2)
     end;
end;

%try to fit to the very beginning and end of the curve this will
%distinguish resistors
[lines(7,1) lines(7,2) lines(7,3) lines(7,4) lines(7,5) lines(7,6) ...
    lines(7,7)] = findlinear([IV(1:100,:);...
    IV(length(IV)-100:length(IV),:)],100,40,1,200,-1);
```

```
%experiments with larger range in Voltage showed that this is a more
%reliable way of determining the actual normal resistance for
%junctions.
%NOTE: this does not apply for shunted curves
%NOTE: The slope here is 1/R but for the sake of confusion I don't call
%it G or anything
Rn = lines(7,2);
Rn_error = lines(7,6);%error from fitting algorithm
%sub gap slope is the average of the two sides of the sub gap slopes
Rsg = (lines(3,2)+lines(4,2))./2;
Rsg_error = (lines(3,6) + lines(4,6))./sqrt(2);

%now check to see if its in fact resistive
 if or(and(((Rsg/Rn)>.7), std(lines(:,3)) <...
         1.5.*mean(lines(:,3))),element=='r')
    if (~supress_output)
         fprintf(' - resistive\n');
    end
    IV_analyze_output = [IV_analyze_output,' - resistive\n'];
    type = 'r';
    status = ' resistive';
    %if its resistive  fit a line to the whole thing
    [a,aerr,chi,yfit]=fitlin(IV);
    %Rsg becomes meaningless
    Rsg=0;
    Rn=a(2);
    Rsg_error=0;
    Rn_error=aerr(2);
    if (plot_things)
```

```
        plot(IV(:,1),yfit,'--r','LineWidth',1)
    end
    %change here to modify definition of shunted.
elseif abs(lines(3,3)-lines(4,3))>(max(IV(:,2))-min(IV(:,2)))./8
    if (~supress_output)
        fprintf(' - shunted\n');
    end
    type = 's';
    status = ' shunted';
    IV_analyze_output = [IV_analyze_output,' - shunted\n'];

    %Quantities defined for processing
    I_knee =abs((lines(4,3)-lines(3,3))./2)./.68;
    %will be reversed to find Ic in junction_finder
    Rn = (lines(1,2)+lines(2,2))./2;
    %this is when shunted resistances are correctly described
    Rsg = (lines(3,2)+lines(4,2))./2;
    %if Rsg and Rn slopes are similar, but not resistive, LEAKY
elseif or(lines(3,2)./lines(1,2)>.55,lines(4,2)./lines(2,2)>.55)
    if (~supress_output)
        fprintf(' - leaky junction\n');
    end
    type = 'l';
    IV_analyze_output = [IV_analyze_output,' - leaky junction\n'];
    status = ' leaky';
else
    %guess a slope for the 3mV spikes based on V and I range
    exp_slope=...
        abs(20*(IV(length(IV),2)-IV(1,2))/(IV(length(IV),1)-IV(1,1)));
```

```
%trying to find max of slope, this is redone in the fitting method
%Done with an averaging method of the five nearest points.
[junk index]=...
    max( slope(Vknee_index_low-100:Vknee_index_low+100)+...
    slope(Vknee_index_low-99:Vknee_index_low+101)+...
    slope(Vknee_index_low-98:Vknee_index_low+102)+...
    slope(Vknee_index_low-101:Vknee_index_low+99)+...
    slope(Vknee_index_low-102:Vknee_index_low+98));
index = index+Vknee_index_low-101;
[junk index]=...
    max(slope(Vknee_index_high-100:Vknee_index_high+100)+...
    slope(Vknee_index_high-99:Vknee_index_high+101)+...
    slope(Vknee_index_high-98:Vknee_index_high+102)+...
    slope(Vknee_index_high-101:Vknee_index_high+99)+...
    slope(Vknee_index_high-102:Vknee_index_high+98));
index = index + Vknee_index_high-101;

%useful for finding out why fitting is going wrong
%plot(IV(Vknee_index_low,1),IV(Vknee_index_low,2),'r+');
%plot(IV(Vknee_index_high,1),IV(Vknee_index_high,2),'r+');

%alot is going on here, see code of findlinear for details
[lines(5,1) lines(5,2) lines(5,3) lines(5,4) lines(5,5) lines(5,6)]...
    = findlinear(IV,Vknee_index_low,2,...
    Vknee_index_low-25,Vknee_index_low+25,exp_slope);
[lines(6,1) lines(6,2) lines(6,3) lines(6,4) lines(6,5) lines(6,6)]...
    = findlinear(IV,Vknee_index_high,2,...
    Vknee_index_high-25,Vknee_index_high+25,exp_slope);
%leaky is also when these peaks aren't steep enough
```

```
if or(((lines(1,2)./lines(5,2))>.5),((lines(2,2)./lines(6,2))>.5))
    if (~supress_output)
        fprintf(' - leaky junction\n');
    end
    type = 'l';
    IV_analyze_output = [IV_analyze_output,' - leaky junction\n'];
    status = ' leaky';
else
    %calculate intersects and errors. error is difference between
    %max allowed by error and the actual value
    V_knee_left=(lines(7,3)-lines(5,3))./(lines(5,2)-lines(7,2));
    V_knee_left_error=...
        abs((lines(7,3)+lines(7,7)+lines(5,7)-lines(5,3))./...
        (lines(5,2)-lines(5,6)-lines(7,6)-lines(7,2))-V_knee_left);
    I_knee_left = lines(7,3)+lines(7,2).*V_knee_left;
    I_knee_left_error=...
        abs((lines(7,3)-lines(5,3)+lines(7,7)+lines(5,7))./...
        (lines(5,2)-lines(7,2)-lines(7,6)-lines(5,6)).*...
        (lines(7,2)+lines(7,6))+lines(7,3)+lines(7,7)-I_knee_left);

    V_bott_left = (lines(3,3)-lines(5,3))./(lines(5,2)-lines(3,2));
    V_bott_left_error =...
        abs((lines(3,3)+lines(3,7)+lines(5,7)-lines(5,3))./...
        (lines(5,2)-lines(5,6)-lines(3,6)-lines(3,2))-V_bott_left);
    I_bott_left = lines(3,3)+lines(3,2).*V_bott_left;
    I_bott_left_error = ...
        abs((lines(3,3)-lines(5,3)+lines(3,7)+lines(5,7))./...
        (lines(5,2)-lines(3,2)-lines(3,6)-lines(5,6)).*...
        (lines(3,2)+lines(3,6))+lines(3,3)+lines(3,7)-I_bott_left);
```

```
V_knee_right=(lines(7,3)-lines(6,3))./(lines(6,2)-lines(7,2));
V_knee_right_error=...
    abs((lines(2,3)+lines(7,7)+lines(6,7)-lines(6,3))./...
    (lines(6,2)-lines(6,6)-lines(7,6)-lines(7,2))-V_knee_right);
I_knee_right = lines(7,3)+lines(7,2).*V_knee_right;
I_knee_right_error=...
    abs((lines(7,3)-lines(6,3)+lines(7,7)+lines(6,7))./...
    (lines(6,2)-lines(7,2)-lines(7,6)-lines(6,6)).*...
    (lines(7,2)+lines(7,6))+lines(7,3)+lines(7,7)-I_knee_right);

V_bott_right=(lines(4,3)-lines(6,3))./(lines(6,2)-lines(4,2));
V_bott_right_error=...
    abs((lines(4,3)+lines(4,7)+lines(6,7)-lines(6,3))./...
    (lines(6,2)-lines(6,6)-lines(4,6)-lines(4,2))-V_bott_right);
I_bott_right=lines(4,3)+lines(4,2).*V_bott_right;
I_bott_right_error=...
    abs((lines(4,3)-lines(6,3)+lines(4,7)+lines(6,7))./...
    (lines(6,2)-lines(4,2)-lines(4,6)-lines(6,6)).*...
    (lines(4,2)+lines(4,6))+lines(4,3)+lines(4,7)-I_bott_right);

%Average I/V_knee to remove offset
I_knee = (I_knee_right-I_knee_left)./2;
I_knee_error = (I_knee_right_error+I_knee_left_error)./sqrt(2);
V_knee = (V_knee_right-V_knee_left)./2;
V_knee_error = (V_knee_right_error+V_knee_left_error)./sqrt(2);

%Average I/V_sg to remove offset
V_sg = (2*V_knee + V_bott_right - V_bott_left)./4;
V_sg_error = (V_knee_error./sqrt(2) +...
    (V_bott_left_error + V_bott_right_error)./(2));
```

```
I_gap = (2*I_knee + I_bott_right - I_bott_left)./4;
I_gap_error = (I_knee_error./sqrt(2) +...
    (I_bott_left_error + I_bott_right_error)./(2));
if (~supress_output)
    fprintf(' - valid junction\n');
end
type = 'j';

%%%%%%%%%%%%%%%%%%%%%%%%%%%%%%%%
kB = .086155;%meV/K
T = 4.2;%K
Delta=(V_knee+V_sg)./4; %meV
Delta_error = (V_knee_error.^2./16+V_sg_error.^2./16).^.5;
Rn_temp = Rn.^-1; %Rn_temp is inverse of slope - kOhm
Rn_error_temp = Rn_error.*Rn_temp.^2;
Ic = (pi * Delta)./(2*Rn_temp).*tanh(Delta./(2*kB*T));
didd =...
    (pi)./(2.*Rn_temp).*tanh(Delta./(2*kB*T))+(pi.*Delta)./...
    (2.*Rn_temp).*(1-tanh(Delta./(2*kB*T)).^2).*(1./(2.*kB.*T));
didr = pi.*Delta)./(2 .* Rn_temp.^2).*tanh(Delta./(2*kB*T));
Ic_error =...
    (Delta_error.^2.*didd.^2 + Rn_error_temp.^2.*didr.^2).^.5;
%%%%%%%%%%%%%%%%%%%%%%%%%%%%%%%%
IV_analyze_output = [IV_analyze_output,' - valid junction\n'];
status = ' valid';
if (plot_things)
    plot(IV(lines(5,4):lines(5,5),1),lines(5,2).*IV(lines...
        (5,4):lines(5,5),1)+lines(5,3),'-r','LineWidth',2)
    plot(V_knee_left,I_knee_left,'ok','LineWidth',2);
    plot(V_bott_left,I_bott_left,'ok','LineWidth',2);
```

```
            plot(IV(lines(6,4):lines(6,5),1),lines(6,2).*IV(lines...
                (6,4):lines(6,5),1)+lines(6,3),'-r','LineWidth',2)
            plot(V_knee_right,I_knee_right,'ok','LineWidth',2);
            plot(V_bott_right,I_bott_right,'ok','LineWidth',2);
            V = axis;
            text(.75.*V(1),.8.*V(4),['I_c = ',...
                num2str(round(Ic.*1000.)./1000),' \pm ',...
                num2str(round(1000.*Ic_error)./1000),' (\muA)'],...
                'FontWeight','bold','FontSize',graphFontSize-2);
            text(.75.*V(1),.6.*V(4),['\Delta = ',...
                num2str(round(Delta.*1000)./1000),' \pm ',...
                num2str(round(1000.*Delta_error)./1000),' (mV)'],...
                'FontWeight','bold','FontSize',graphFontSize-2);
        end
    end
end
%invert everything because the slope is 1/R
%error is non-trivial
Rn = Rn.^-1;
Rn_error = Rn_error.*Rn.^2;
if Rsg ~= 0
    Rsg = Rsg.^-1;
    Rsg_error = Rsg_error.*Rsg.^2;
end
if (plot_things)
    V = axis;
    plot(IV(1:length(IV),1),...
        lines(7,2).*IV(1:length(IV),1)+lines(7,3),'--r')

    %display resistances in smallest units
```

```
        if Rn<.1
            Rn_units = ' (\Omega)';
            Rn_mult = 1000;
        else
            Rn_units = ' (k\Omega)';
            Rn_mult = 1;
        end
        if abs(Rsg)<.1
            Rsg_units = ' (\Omega)';
            Rsg_mult = 1000;
        else
            Rsg_units = ' (k\Omega)';
            Rsg_mult = 1;
        end
        text(-.5,.6.*V(3),['R_{n} = ',...
            num2str(round(Rn_mult*Rn*1000)/1000),' \pm ',...
            num2str(round(Rn_mult*1000*Rn_error)/1000),Rn_units],...
            'FontWeight','bold','FontSize',graphFontSize-2);
        if (type~='r')
            text(-.5,.8.*V(3),['R_{sg} = ',...
                num2str(round(Rsg_mult*Rsg*1000)/1000),' \pm ',...
                num2str(round(Rsg_mult*1000*Rsg_error)/1000),Rsg_units],...
                'FontWeight','bold','FontSize',graphFontSize-2);
        end
    end
end

if (plot_things)
    if shifted
        status = ['noisy ',status];
```

```
    end
    title([word,' - ',status],...
        'interpreter','none','FontWeight','bold','FontSize',graphFontSize);
end
%this plot is saved in junction_finder, this function doesn't know anything
%about the wafer or die.

%%%%%%%%%%%%%%%%%%%%%%%%%%%%%%%%%%%%%%%%%%%%%%%%%%%%%%%%%%%%%%%%%%%%%%%%%%%
%%%%%%%%%%%%%%%%%%%%%%%%%%%%%%%%%%%%%%%%%%%%%%%%%%%%%%%%%%%%%%%%%%%%%%%%%%%


function [trimmed] = trim(a)
%there is an intentional error here, it will take the furthest point in the
%trace that matches the intial and cut off from there. Because the traces
%are generally increasing this is fine and it only effects the open cases.
%Because of this, modifying this might have bad effects on some of the
%determination in IV_analyze specifically for open cases.
len = length(a); init = a(1,2); beg = 1; endv = a(len,2); stop =
len;
if (init ~= 0)      %if the initial value is 0, means there is no data
    for i=4:len
        if (a(i,2) == init)
            beg = i;
            %break;
        end
    end
    for i=1:len-4
        if ( a(i,2) ~= endv )
            stop = i+1;
           % break;
```

```
        end
    end
end trimmed=a(beg:stop,:);
%%%%%%%%%%%%%%%%%%%%%%%%%%%%%%%%%%%%%%%%%%%%%%%%%%%%%%%%%%%%%%%%%%%%%%%%%%%%
%%%%%%%%%%%%%%%%%%%%%%%%%%%%%%%%%%%%%%%%%%%%%%%%%%%%%%%%%%%%%%%%%%%%%%%%%%%%

function [mid slope intercept start_index end_index slope_error ...
    intercept_error] = ...
    findlinear(IV,mid,dist,left_bound,right_bound,exp_slope)



%an exp_slope that is not -1 means that the program will recenter around
%the that when fitted to its neighoring points is the steepest. This is
%exclusively for fitting the 3mV peaks in JJ traces
if exp_slope ~= -1

    for i=1:right_bound-left_bound-dist-dist
        [x1,x2,x3,x4] = fitlin(IV(i+left_bound-1:i+left_bound+dist+dist,:));
        slope(i)=x1(2);
    end



    [junk index]=max(slope);
    mid=index+left_bound+dist-1;

    %good for finding if the program is doing something wrong
    %plot(IV(mid,1),IV(mid,2),'r+');
    range = round((right_bound-left_bound)/2);
    right_bound = mid + range;
    left_bound = mid - range;
```

```
    %recall program but don't allow recentering
    [mid slope intercept start_index end_index slope_error ...
        intercept_error] = findlinear(IV,mid,dist,left_bound,right_bound,-1);
else
    trials = 5;
    %number of iterations to find the ideal line
    %I've found 3 to be enough to minize the error
    for i=1:trials

        posspace = right_bound - mid;
        negspace = mid-1-left_bound;

        posdist = dist;
        negdist = dist;

        %prevents it from thinking some very small number is the right
        %distance
        err = 50000.*ones(1,posspace);

        %check the whole space for the error, the quantity to be minimized
        %is the average residual of the line.
        for posdist=dist:posspace
            [a,aerr,chisq,yfit] = fitlin(IV(mid-negdist:mid+posdist,:));
            err(posdist) = mean(abs(yfit-IV(mid-negdist:mid+posdist,2)));
        end;
        [junk1,minima]=min(err);
        posdist = minima;
        clear err;
```

```
        %repeat for the negetive direciton
        err = 50000.*ones(1,negspace);
        for negdist=dist:negspace
            [a,aerr,chisq,yfit] = fitlin(IV(mid-negdist:mid+posdist,:));
            err(negdist)=mean(abs(yfit-IV(mid-negdist:mid+posdist,2)));

        end;
        [junk1,minima]=min(err);
        negdist =  minima;
        clear err;
        %needs to be iterated because minizing each direction can change
        %the solution
    end
    %final fit of chosen points
    [a,aerr,chisq,yfit] = fitlin(IV(mid-negdist:mid+posdist,:));
    slope = a(2);
    intercept = a(1);
    slope_error = aerr(2);
    intercept_error = aerr(1);
    start_index = mid-negdist;
    end_index = mid+posdist;
end
%%%%%%%%%%%%%%%%%%%%%%%%%%%%%%%%%%%%%%%%%%%%%%%%%%%%%%%%%%%%%%%%%%%%%%%%%%%
%%%%%%%%%%%%%%%%%%%%%%%%%%%%%%%%%%%%%%%%%%%%%%%%%%%%%%%%%%%%%%%%%%%%%%%%%%%

function [a,aerr,chisq,yfit] = fitlin(IV)
%simple linear fitting algorithm
x = IV(:,1); y = IV(:,2);

%imported from IV_analyze as defined there
```

```
global inst_error; sig = zeros(length(y),1)+inst_error;

term1=sum(1./sig.^2); term2=sum(x.^2./sig.^2); term3=sum(y./sig.^2);
term4=sum(x.*y./sig.^2); term5=sum(x./sig.^2);

delta=term1*term2-term5^2;

%a=[intercept slope]
a(1)=(term2*term3-term5*term4)/delta;
a(2)=(term1*term4-term5*term3)/delta;

%aerr=[intercept_error slope_error]
aerr(1)=sqrt(term2/delta); aerr(2)=sqrt(term1/delta);

%yfit is the y value corresponding to each x value
yfit = a(1) + a(2)*x;

%chisq is non-reduced chi squared value of fit
chisq = sum(((y-a(1)-a(2)*x)./sig).^2);
%%%%%%%%%%%%%%%%%%%%%%%%%%%%%%%%%%%%%%%%%%%%%%%%%%%%%%%%%%%%%%%%%%%%%%%%%%%
%%%%%%%%%%%%%%%%%%%%%%%%%%%%%%%%%%%%%%%%%%%%%%%%%%%%%%%%%%%%%%%%%%%%%%%%%%%

function [IV candidate] = cleanup(IV, start_point, end_point);
%this is a function to seperate top and bottom parts of noisy IV traces
%which is due to the averaging technique of the oscilliscope
%to be done on one leg of the curve at a time.

top = max(IV(start_point:end_point,2)); bot =
min(IV(start_point:end_point,2));
```

```
align = zeros(end_point-start_point,1); part1=[]; part2=[];

%assigning each point to either top or bottom
for i=1:end_point-start_point
    if abs(IV(i+start_point,2)-top)<abs(IV(i+start_point,2)-bot)
        align(i)=1;
        part1(length(part1)+1)=IV(i+start_point,2);
    else
        align(i)=-1;
        part2(length(part2)+1)=IV(i+start_point,2);
    end
end

%look at each side
mean1=mean(part1); count1=length(part1); mean2=mean(part2);
count2=length(part2);

%normalize to the size with the most points
if count1>count2
    align = align - 1;
else
    align = align + 1;
end

%take into account min distance between pixels
global inst_error;
candidate = 4; %tolerance of 3 pixels in dead region
%i did this an unorthodox way, mainly to be difficult but also because more
%than the threshold of hits also needs to remain disallowed
for i=1:end_point-start_point
```

```
    %for each pixel in dead region take away from tolerance
    if and(IV(i+start_point,2)>mean2-inst_error+.45*(mean1-mean2),...
            IV(i+start_point,2)<mean2+inst_error+.55*(mean1-mean2))
        candidate = candidate./2;
        candidate = floor(candidate);
    end
end

if and(candidate,and(length(part1)>1,length(part2)>1))
    %if its divided, add the difference in means to the less populated
    %side, hopefully making them one line.
    for i=1:end_point-start_point
        IV(i+start_point,2)=IV(i+start_point,2)-(mean1-mean2)*align(i)./2;
    end
end
```

Appendix C

Design Schematics

PRODUCED BY AN AUTODESK EDUCATIONAL PRODUCT

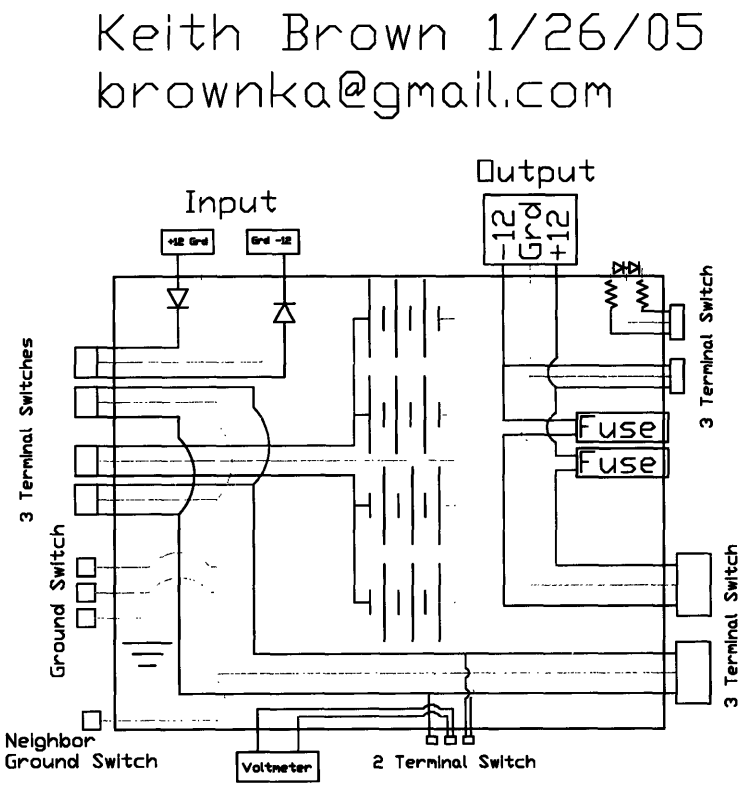

PRODUCED BY AN AUTODESK EDUCATIONAL PRODUCT

PRODUCED BY AN AUTODESK EDUCATIONAL PRODUCT

PRODUCED BY AN AUTODESK EDUCATIONAL PRODUCT

Figure C-1: Electrical schematic of the battery circuit. A single voltmeter can be switched to read either polarity. Each battery circuit ground can be connected to the neighboring circuit's ground.

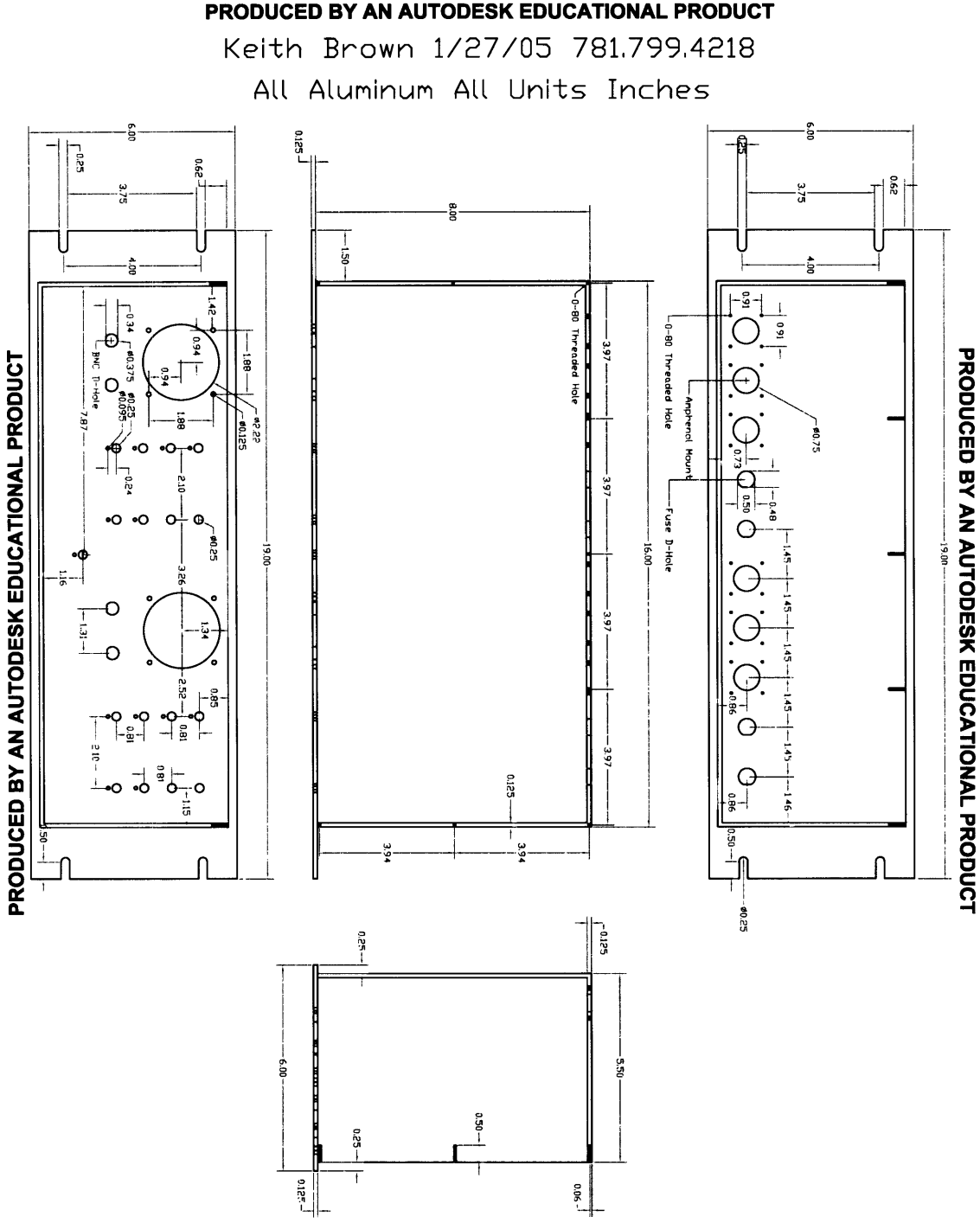

Figure C-2: Design schematic of the physical battery box. Two complete batteries fit inside each box. A simple aluminum lid (not pictured) is attached to the top of the box to ensure electrical shielding. The box is designed to fit in a standard rack mount.

PRODUCED BY AN AUTODESK EDUCATIONAL PRODUCT

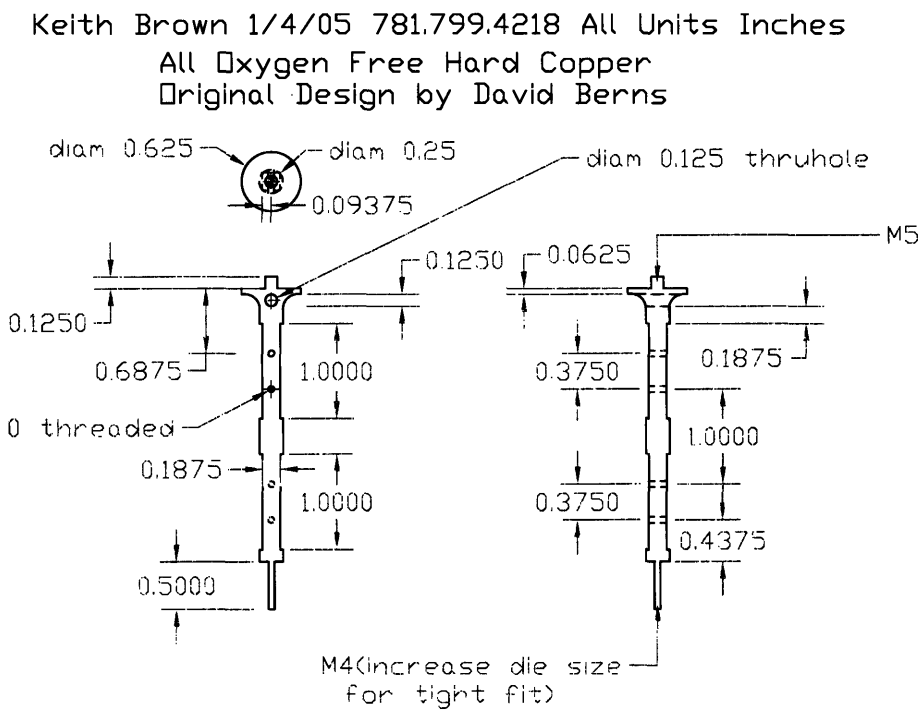

PRODUCED BY AN AUTODESK EDUCATIONAL PRODUCT

PRODUCED BY AN AUTODESK EDUCATIONAL PRODUCT

PRODUCED BY AN AUTODESK EDUCATIONAL PRODUCT

Figure C-3: Design schematic of the thermal finger that holds the chip in place. The chip attaches to a small mount that screws onto the end of the finger. This both holds the chip in place and maintains a good thermal connection. The four holes through the finger are where the copper powder filters attach.

PRODUCED BY AN AUTODESK EDUCATIONAL PRODUCT

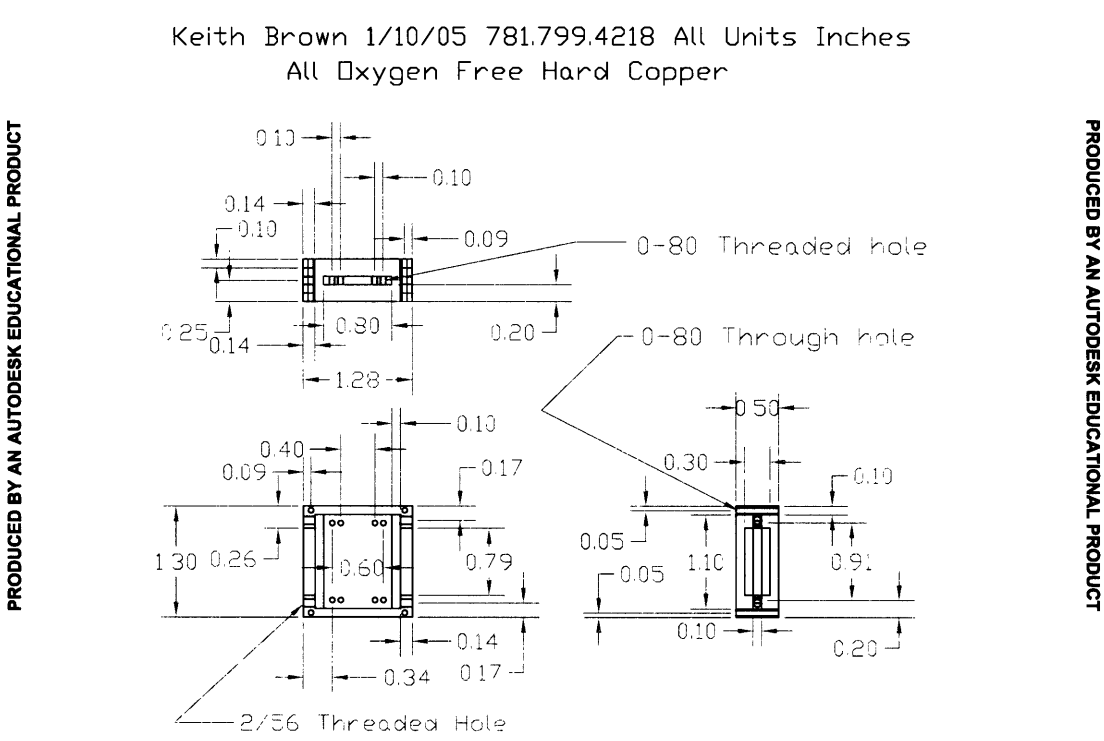

PRODUCED BY AN AUTODESK EDUCATIONAL PRODUCT

PRODUCED BY AN AUTODESK EDUCATIONAL PRODUCT

PRODUCED BY AN AUTODESK EDUCATIONAL PRODUCT

Figure C-4: Design schematic for the box that holds the RC filter. A mini D-sub plug attaches to each side of the box. Two removable lids (not pictured) attach to the top and bottom for access to the circuit boards. The circuit boards mount back to back in the middle of the device for space conservation.

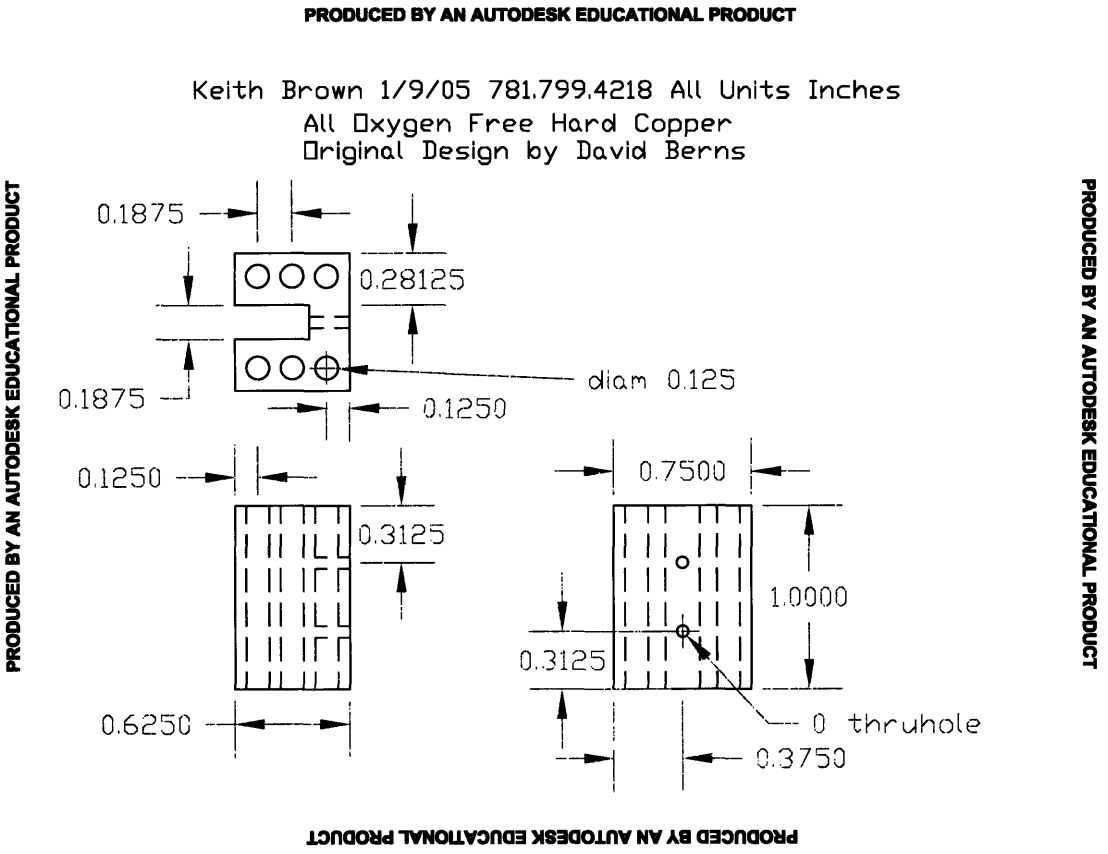

Figure C-5: Design schematic for the copper powder filters. Each unit holds six copper powder filters, each with a twisted pair running though it. The filters attach to the thermal finger via two screws.

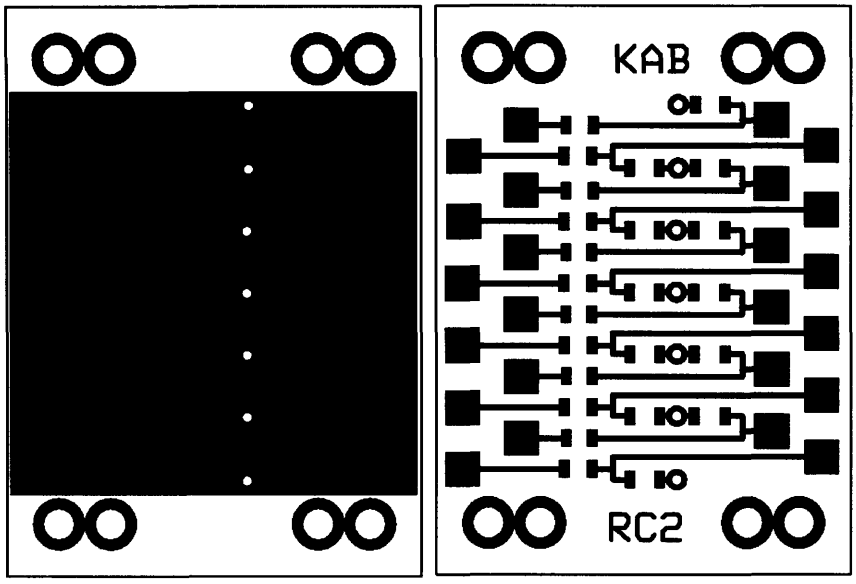

Figure C-6: PC board design for the RC low-pass filter. Each of twelve channels has room for a resistor in series and a capacitor to ground. The back is a ground plate that rests on the device box.

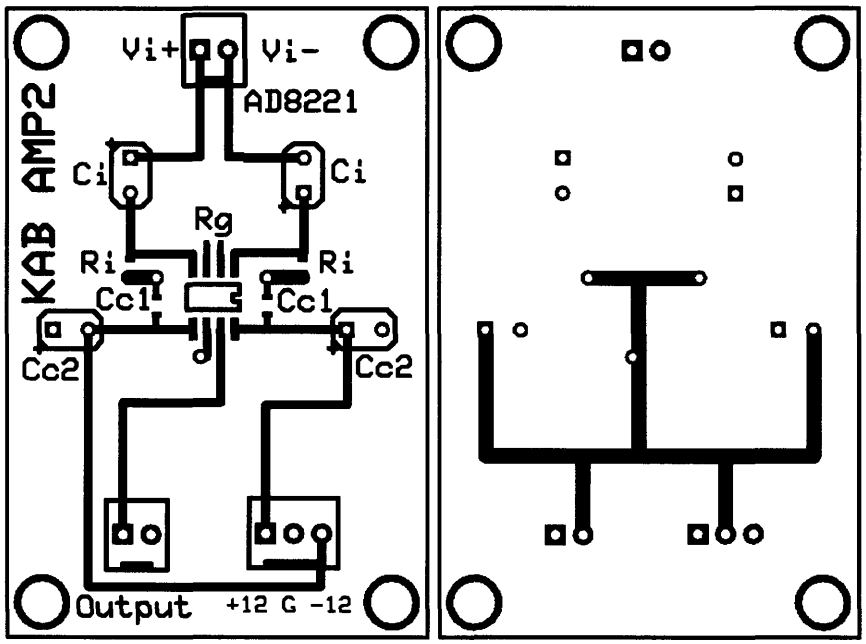

Figure C-7: PC board design for the amplifier circuit. In addition to decoupling capacitors, the design also features single pole RC high-pass filters on the inputs. This eliminates DC noise. External connections enter through Molex connectors soldered onto the surface.

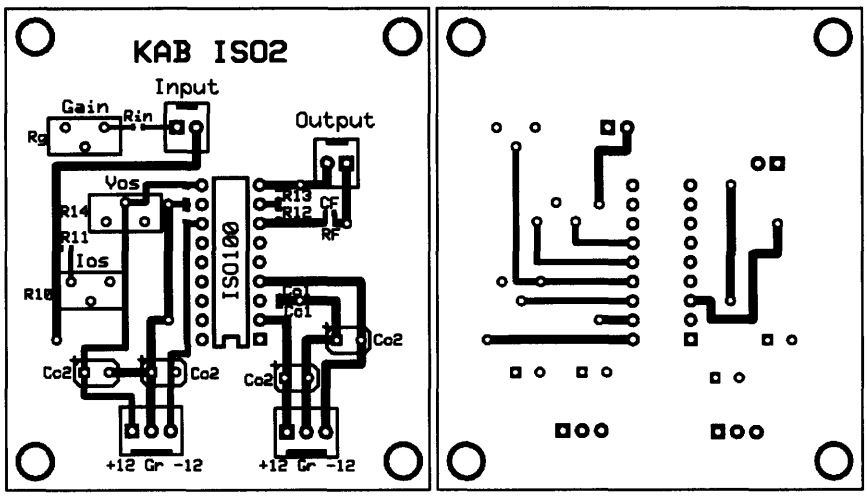

Figure C-8: PC board design for the optical isolation circuit. The circuit has a total of eight decoupling capacitors. There are three potentiometers used to trim various characteristics of the device. The chip itself fits inside an 18-pin dip connection for easy interchange.

Bibliography

Bibliography

[1] B.D. Josephson, Phys. Lett. **1** 7 251(1962)

[2] T.Van Duzer, C.W. Turner, *Principles of Superconductive Devices and Circuits*, 1st ed. (Elevier North Holland 1981).

[3] J.R. Kirtley, *et. al.*, App. Phys. Lett. **66** 9, 1138(1995).

[4] S.P. Kwon, *et. al.*, APS Meeting Abstracts, March 20001(2003).

[5] M.A. Espy, *et. al.*, IEEE Trans. on App. Superconductivity **15** 2, 635(2005).

[6] T.P. Orlando, *et. al.*, Phys. Rev. B **60**, 15398 (1999).

[7] Y. Makhlin, *et. al.*, Rev. of Mod. Phys. **73** April 357(2001).

[8] P. Jarillo-Herrero *et. at.*, Nature **439**, 953 (2006).

[9] S. Raghavan, *et. al.*, Phys. Rev. A **59** 620(1999).

[10] S. Giovanazzi, Phys. Rev. Lett. **84** 4521(2000).

[11] G.I. Rochlin, Phys. Rev. **153** 513(1967).

[12] K.V.R.M. Murali, *et. al.*, Phys. Rev. Lett. **93** 087003(2004).

[13] J.C. Lee, *et. al.*, IEEE Transactions on Applied Superconductivity, **15** 2(2005).

[14] W.D. Oliver, *et. al.*, Science **310** 5754(2005).

[15] M. Tinkham, *Introcution to Superconductivity*, reprint (Robert E Krieger Publishing Co. 1980).

[16] J. Bardeen, L.N. Cooper, J.R. Schrieffer, Phys. Rev. **108** 1175(1957).

[17] C. Kittel, *Introduction to Solid State Physics*, 8th ed. (John Wiley and Sons, Inc 2005).

[18] D.J. Griffiths, *Introduction to Quantum Mechanics*, 2nd ed. (Prentice Hall 2005).

[19] A. Ambegoakar, A. Baratoff, Phys. Rev. Lett. **10** 468(1963).

[20] M. Fiske, Rev. Mod. Phys. **36**, 221 (1964).

[21] R. Feynman, *The Feynman Lectures in Physics*, (Pearson 1965).

[22] J. Mannhart, *et. al.*,Jornal of Low Temp. Phys. **70** 5/6 (1988).

[23] R. Vaglio, Journal of Low Temp. Phys. **25** 3/4 (1976).

[24] D.J. Griffiths, *Introduction to Electrodynamics*, 3rd ed. (Prentice Hall 1999).

[25] J.W. Hafstrom, M.L.A. MacVicar, Phys. Rev. B **2**, 4511 (1970).

[26] D.K. Finnemore, T.F. Stromberg, C.A. Swenson, Phys. Rev. **149**, 231(1966).

[27] P.R. Bevington, D.K. Robinson *Data Reduction and Error Analysis for the Physical Sciences*, 2rd ed. (McGraw-Hill 1992).

[28] C.L. Foden, *et. al.*, Phys. Rev. B, **47** 6, 3316(1993).

[29] N. Agraït, *et. al.*, Phys. Rev. B. **47** 18, 12345(1993).

[30] A.C. Rose-Innes, *Low Temperature Laboratory Techniques*, 2nd ed. (Crane Russak and Co. Inc. 1973).